Subdiffusion and localization in the one-dimensional trap model

E. M. Bertin and J.-P. Bouchaud
Commissariat à l'Énergie Atomique, Service de Physique de l'État Condensé, 91191 Gif-sur-Yvette Cedex, France
(Received 23 October 2002; published 27 February 2003)

We study a one-dimensional generalization of the exponential trap model using both numerical simulations and analytical approximations. We obtain the asymptotic shape of the average diffusion front in the subdiffusive phase. Our central result concerns the localization properties. We find the dynamical participation ratios to be finite, but different from their equilibrium counterparts. Therefore, the idea of a partial equilibrium within the limited region of space explored by the walk is not exact, even for long times where each site is visited a very large number of times. We discuss the physical origin of this discrepancy, and characterize the full distribution of dynamical weights. We also study two different two-time correlation functions, which exhibit different aging properties: one is ''sub aging'' whereas the other one shows ''full aging,'' therefore, two diverging time scales appear in this model. We give intuitive arguments and simple analytical approximations that account for these differences, and obtain new predictions for the asymptotic (short-time and long-time) behavior of the scaling functions. Finally, we discuss the issue of multiple time scalings in this model.

DOI: 10.1103/PhysRevE.67.026128 PACS number(s): 02.50.−r, 75.10.Nr, 05.20.−y

I. INTRODUCTION

A lot of efforts have been devoted to the theoretical study of aging phenomena in the past decades [1–3]. Spin glass models, which exhibit a very rich phenomenology, have been widely studied theoretically both using analytical techniques for the mean field models, or by numerical simulations in the finite dimensional cases. Besides these microscopic spin models, a simpler but phenomenological picture, the ''trap model,'' has been proposed in order to describe the phase space dynamics in a coarse-grained manner [4]. This model seems to capture, at least qualitatively, some of the physics involved in the aging dynamics of several systems beyond spin glasses, such as fragile glasses [5–7], soft glassy materials [8,9], granular materials [10], pinning of extended defects (such as domain walls, vortices, etc.) [11]. This trap model has been studied mainly in its fully connected (or ''mean field'') version [12–14], which has recently been shown to describe exactly the long-time dynamics of the random energy model when the distribution of trap depth is exponential [15]. This version of the mean field model already exhibits a number of interesting features, such as a transition between a stationary, ''liquid'' phase, and an aging ''glassy'' phase, violation of the fluctuation dissipation relation [16], and dynamical ultrametricity [17,18]. In the glassy phase, the dynamics is strongly intermittent, since most of the time nothing happens, whereas the active periods appear in bursts which become less and less frequent as time elapses. Several recent experiments suggest that such an intermittency is indeed present in glassy systems [19–21], or in atomic physics [22–24].

The finite-dimensional generalization of this model has already been studied many years ago [25–28], but only one-time quantities (not well suited to study aging) were considered. These aging properties were addressed only recently in Refs. [14,29], and, from a more rigorous point of view, in Refs. [30,31]. One expects that in dimensions $d>2$, the trap model will have properties qualitatively similar to the fully connected case, since each site is visited by the walk a finite number of times. In lower dimensions $d\leqslant 2$, the correlations induced by the multiple visits of the walks to a given site is expected to lead to qualitative changes. It was for example shown in Ref. [29] that some quantities exhibit *subaging* properties, i.e., decay on a time scale that scale with the waiting time t_w as t_w^ν with $\nu<1$. Because of the limited number of accessible sites, one might also expect interesting properties such as *dynamical localization*, which means that there is a finite probability that k independent particles sit on the very same site, even after a very long waiting time t_w. Such a dynamical localization was first established by Golosov in the context of the Sinai model [32] and extended to the biased case in Ref. [33], and more recently proven rigorously for the one-dimensional trap model in Ref. [30].

In this paper, we present a detailed study of the one-dimensional (nonbiased) trap model, using both numerical simulations and analytical approximations. In the first section, we focus on the scaling form of the average ''diffusion front'' $\langle p(x,t)\rangle$ in the subdiffusive, non-Gaussian phase, for which no analytical results are (to our knowledge) available. We present some scaling arguments and approximation schemes to account for our numerical data. We then discuss the idea of partial equilibrium in this model, which can be explored in details through the distribution of dynamical weights. The moments of this distribution are the usual ''participation ratios'' that characterize the localization properties of the measure. Perhaps surprisingly, these localization indicators are indeed finite (as first shown in Ref. [30]), but different from their static counterparts. We discuss in detail the origin of this difference, and try to characterize quantitatively the distribution of dynamical weights. In the last section, we study the aging behavior of two different correlation functions, which exhibit different scaling properties, meaning that two different time scales, t_w^ν and t_w, appear in this model. We again develop intuitive arguments and simple analytical approximations to understand these differences, and obtain new predictions for the asymptotic behavior of the scaling functions, which are found to be in excellent agreement with the numerics. Finally, we discuss the possible existence of multiple time scalings in this model (as can

happen in spin glasses [17] or in a generalization of the trap model [29]).

II. THE ONE-DIMENSIONAL TRAP MODEL: ANOMALOUS DIFFUSION

A. Definition of the model

Consider a one-dimensional lattice, and define on each site i a quenched random variable $E_i>0$ chosen from a distribution $\rho(E)$. E_i has to be interpreted as the energy barrier that the particle (the walker) has to overcome in order to leave the site. The dynamics is chosen to be activated with temperature T, which means that the escape rate w_i of site i is given by $w_i=\Gamma_0 e^{-E_i/T}$, where Γ_0 is a microscopic frequency scale. Once that particle has escaped the trap, it chooses one of the two neighboring sites, with probability q_- for the left one and $q_+=1-q_-$ for the right one. The ''directed'' case $q_+=1$ is quite simple to analyze analytically, since each is visited once—see Refs. [34,28,33]. The case $q_+=1/2$ that we study in the following is much more subtle since each site is visited a large number of times, inducing long range correlations in the hopping rates seen by the walker. (Note that as soon as $q_+\neq 1/2$, one expects the large time properties of the walk to be the same as in the fully directed case [33].)

An important remark has to be done at this point, while all numerical studies were done specifically with the model described above, where hopping is constrained to nearest neighbor sites, both the analytical calculations and the simplified arguments presented in this paper are expected to apply to the more general case where hopping is only constrained to have a finite range ℓ_{hop}.

For the purpose of heuristic arguments and Monte Carlo studies, it is interesting to study the trapping time τ of the particle on each site. Once the transition rates w_i are given, τ is a random variable with a (site dependent) distribution $p_i(\tau)=w_i e^{-w_i\tau}$, of mean $\tau_i=w_i^{-1}$. If we choose an exponential density of trap depths, $\rho(E)=(1/T_g)e^{-E/T_g}$, then the distribution of τ_i's over the different sites is a power law:

$$\psi(\tau)=\frac{\mu\hat{\tau}_0^{\mu}}{\tau^{1+\mu}} \qquad (\tau\geqslant\hat{\tau}_0), \tag{1}$$

where $\mu=T/T_g$ is the reduced temperature, and $\hat{\tau}_0\equiv\Gamma_0^{-1}$. For $T>T_g$, this distribution has a finite average value $\langle\tau\rangle=\hat{\tau}_0/(\mu-1)$. This corresponds to usual diffusion and stationary dynamics, with a diffusion constant $D=a^2/\langle\tau\rangle$, where a is the lattice spacing. On the contrary, for $T\leqslant T_g$, the first moment of the distribution diverges, diffusion becomes anomalous and aging effects are expected. A dynamical phase transition takes place at T_g, as in the fully connected model. However, new properties emerging from the nontrivial spatial structure of the model are expected.

B. Disorder induced subdiffusion: A scaling argument

We first give a simple scaling argument (proposed in Refs. [25,35,28]) that yields a subdiffusive behavior for the one-dimensional trap model introduced above. In the following, we shall take a is the unit of length, as well as Γ_0^{-1} as the time unit. Roughly speaking, a typical random walk starting from a given initial site has visited, after N steps, of the order of $\sqrt{N}$ sites (which implies a typical displacement $\xi\sim\sqrt{N}$). Each site is visited around $\sqrt{N}$ times. So the time t elapsed can be written as

$$t\sim\sqrt{N}\sum_{i=-\sqrt{N}}^{\sqrt{N}}\tau_i. \tag{2}$$

Since the sum of M independent random variables distributed according to Eq. (1) grows as $M^{1/\mu}$, we get

$$t\sim\sqrt{N}^{1+(1/\mu)}\sim\xi^{1+(1/\mu)}. \tag{3}$$

Inverting this relation leads to the following subdiffusive behavior:

$$\xi(t)\sim t^{\mu/(1+\mu)}. \tag{4}$$

Note that the above argument holds only in the long-time limit, which is defined by the condition $\xi(t)\gg\ell_{hop}$. This result was also obtained by Machta [27], using real space renormalization group arguments. The same behavior also holds for the *random barrier* model with a broad distribution of barrier heights which, in one dimension, is expected to be equivalent to the trap model, as far as diffusion properties are concerned [28]. For this model, the average probability of being on the initial site can be exactly computed, and decays as $1/t^{\mu/(1+\mu)}=1/\xi(t)$, in agreement with the above result. The exponent $\mu/(1+\mu)$ is also in very good agreement with numerical results [29].

The case $\mu=1$ is special since logarithmic corrections come into play. Extending the above argument leads to

$$\xi(t)\sim\sqrt{\frac{t}{\ln t}} \quad (\mu=1), \tag{5}$$

whereas for $\mu>1$ one recovers $\xi(t)\sim\sqrt{t}$.

Calling $P_i(t)$ the probability to be on site i after time t, starting from site $i=0$ at time $t=0$, a spatial probability density $p(x,t)$ can be introduced through the relation $P_i(t)=a\,p(ia,t)$. One expects the disordered average diffusion front $\langle p(x,t)\rangle_\tau$ to take for large times the following scaling form:

$$\langle p(x,t)\rangle_\tau=\frac{1}{\xi(t)}f\left(\frac{x}{\xi(t)}\right), \tag{6}$$

where $\xi(t)$ is given by Eq. (4), $f(\cdot)$ is a continuous scaling function and $\langle\cdots\rangle_\tau$ stands for the average over the quenched trapping times τ_i. However, the full scaling function $f(\cdot)$ is, to our knowledge, not known. Only the value of $f(0)$ in the dual ''barrier'' model was obtained in Ref. [26]. Before studying more subtle issues, we have investigated this question both analytically and numerically.

C. The average diffusion front

For a system without disorder, or in the case $\mu>1$ where the average trapping time $\langle\tau\rangle$ is finite, the central limit theorem tells us immediately that the diffusion front becomes Gaussian at large times:

$$\langle p(x,t)\rangle_\tau = \frac{1}{\sqrt{2\pi Dt}}\exp\left(-\frac{x^2}{2Dt}\right), \tag{7}$$

where $D=a^2/\langle\tau\rangle$ is the diffusion constant, a being the lattice spacing, so that $D\propto(\mu-1)$ when $\mu\to1^+$. In the case $\mu\leqslant1$, a modified space-time scaling is expected, as argued in the preceding section, as well as a non-Gaussian diffusion front.

We have developed simple approximation schemes (that we expect to become exact in the limits $\mu\to1$ and $t\to\infty$) to compute $\langle p(x,t)\rangle_\tau$ analytically. The calculations are reported in Appendix A. We find that $\langle p(x,t)\rangle_\tau$ can indeed be written as Eq. (6) with $\xi(t)$ given by Eq. (4). The asymptotic shape of $f[\zeta=x/\xi(t)]$ can furthermore be computed in the limits $\zeta\to0$ and $\zeta\to\infty$. We find

$$f(\zeta)\approx f_\infty|\zeta|^\alpha\exp(-b|\zeta|^\beta),\quad |\zeta|\to\infty, \tag{8}$$

$$f(\zeta)\approx f_0-f_1|\zeta|^\mu-f_2|\zeta|^\gamma,\quad |\zeta|\to0, \tag{9}$$

where $\alpha=(\mu-1)/2$, $\beta=1+\mu$ and $\gamma=\min(2,1+2\mu)$. The constants f_0, f_1, f_2, f_∞, and b are μ dependent numbers that we can also compute in the Appendix [see Eqs. (A26) and (A33)].

In the case $\mu=1$, we find, using the same approximation (which we now believe is exact), that ζ is given by $x\sqrt{\ln x/t}\approx x\sqrt{\frac{1}{2}\ln t/t}$, and that $f(\zeta)$ is exactly Gaussian, as for the normal case $\mu>1$. More precisely, one finds for the diffusion front, in the limit $t\to\infty$:

$$\langle p(x,t)\rangle_\tau \simeq \sqrt{\frac{\ln t}{4\pi t}}\exp\left(-\frac{x^2}{4t}\ln t\right). \tag{10}$$

We have tested numerically the validity of the scaling relation Eq. (6), for several values of μ. The plot of $\xi(t)\langle p(x,t)\rangle$ as a function of $x/\xi(t)$, for different values of t shows a rather good collapse (Fig. 1). The curves collapse well for $\mu=0.2$ and 0.5, even if for $\mu=0.2$ data is more noisy. However, finite-time corrections become stronger as μ approaches 1. This is expected: subleading corrections to scaling can be shown to become negligible only in the limit, where $t^{(1-\mu)/(1+\mu)}\gg1$. For $\mu=0.9$ and $t=10^5$, however, this parameter is only ≈1.8. Therefore, we expect that the $\mu=0.9$ data will actually be strongly affected by the vicinity of $\mu=1$, which plays the role of a critical point.

In Fig. 2 we show the scaling functions for $\mu=0.5$, 0.8, and 0.9 obtained by extrapolating to $t=\infty$ the scaling curves obtained at finite t. We actually plot $f(\zeta)/\zeta^\alpha$ as a function of ζ^β in a semilog plot, in order to test directly the asymptotic form given by Eq. (8). Note that the approximation is supposed to be valid only for μ close to 1, but seems to work well even for rather small values of μ, like $\mu=0.5$. Also

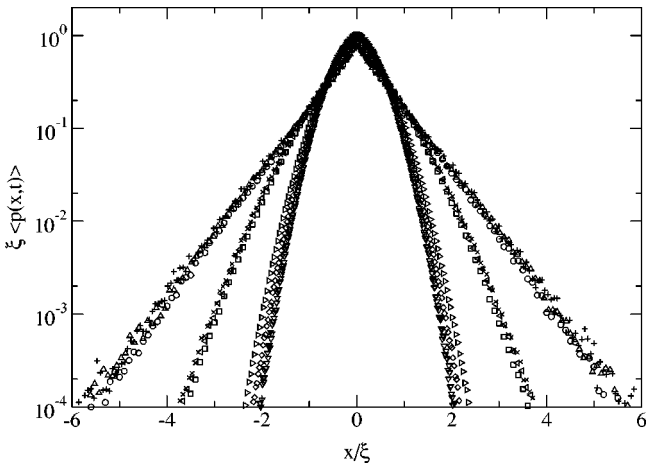

FIG. 1. Plot of $\xi(t)\langle p(x,t)\rangle$ versus $x/\xi(t)$ for different temperatures and different times. Data were obtained by Monte Carlo simulations on the model with fixed trapping times. Upper curves—$\mu=0.2$, and $t=10^6(\bigcirc)$, $10^8(\triangle)$, $10^{10}(+)$; middle curves—$\mu=0.5$ and $t=10^3(\square)$, $10^4(\triangleleft)$, $10^5(\times)$; lower curves—$\mu=0.9$ and $t=10^3(\triangleright)$, $10^4(\diamond)$, $10^5(\triangledown)$.

shown are the analytic predictions, with the computed numerical values of the constants f_∞ and b. We see that the agreement is quite reasonable, and actually suggests that the value $\beta=1+\mu$ is probably exact. For $\mu=0.9$, critical corrections become important and the predicted slope is not as good as for $\mu=0.8$, but the exponent $1+\mu$ seems to be correct.

Data corresponding to $\mu=1$ are shown in Fig. 3. It is actually necessary to take into account a finite-time correction in this case, replacing $\ln t$ by $\ln(\Gamma t)$, where Γ is an unknown constant that has to be fitted. This correction is natu-

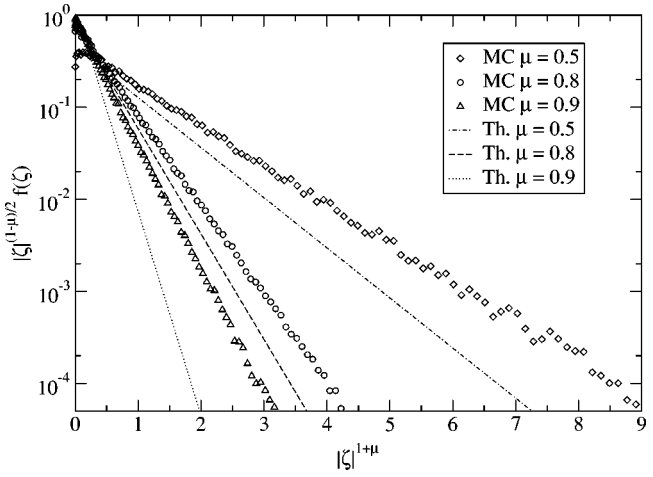

FIG. 2. Plot of $|\zeta|^{(1-\mu)/2}f(\zeta)$ versus $|\zeta|^{1+\mu}$ for $\mu=0.5(\diamond)$, $0.8(\bigcirc)$, and $0.9(\triangle)$, obtained by an infinite-time extrapolation of the Monte Carlo data. The analytical prediction, using the approximation valid for μ close to 1, is also shown for the same values of μ (lines). The predicted exponent $|\zeta|^{1+\mu}$ is in good agreement with the numerics, since data appear to be linear in this representation. The prediction for b—see Eq. (8)—is in best agreement with the Monte Carlo data for $\mu=0.8$.

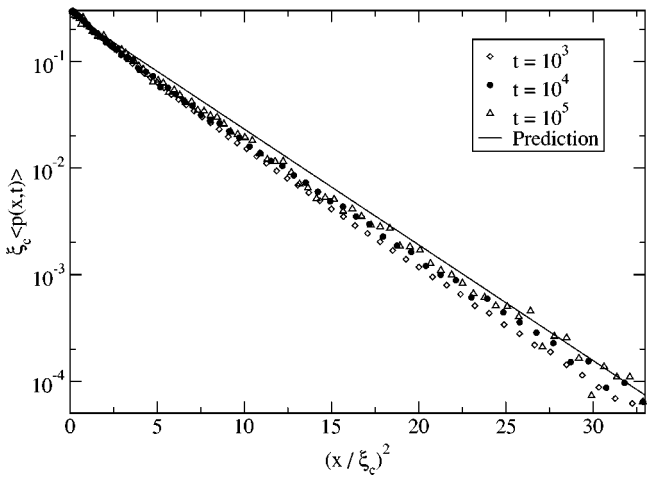

FIG. 3. Plot of $\xi_c(t)\langle p(x,t)\rangle_\tau$ versus $[x/\xi_c(t)]^2$ for $\mu=1$ and times $t=10^3$ ($\diamond$), 10^4 ($\bullet$), and 10^5 ($\triangle$); $\xi_c(t)$ is the critical coherence length, defined as $\xi_c(t)=[t/\ln(\Gamma t)]^{1/2}$, where Γ is fitted on the $t=10^4$ curve. The data points seem to converge at large times towards the asymptotic Gaussian form predicted by Eq. (10) (line).

ral, as can be shown by the structure of the subleading terms. Fitting Γ on data corresponding to $t=10^4$ leads to $\Gamma \simeq 1.64$. One sees that for large x, the slope is then found to be the same for the three-times simulated.

We have also tested the small ζ region. For $\mu=0.5$, the $\sqrt{|\zeta|}$ singularity predicted by our approximation—see Eq. (8)—is rather convincing. However, as μ increases towards 1, the coefficient f_1 of $|\zeta|^\mu$ decreases towards zero. The next leading term becomes important and one indeed observes an effective singularity with an exponent intermediate between μ and 2: we find this exponent to be ≈ 1.6 for $\mu=0.8$ and ≈ 1.8 for $\mu=0.9$.

III. PARTIAL EQUILIBRIUM AND LOCALIZATION

The one-dimensional diffusion problem is interesting because, as mentioned above, each site is visited by the walk a large number of times. A natural idea is therefore that at time t, the probability $P_i(t)$ to find the particle at site i should be very similar to the *equilibrium* distribution restricted to an interval of finite length $\propto \xi(t)$. More precisely, we can expect that $P_i(t)$ can be written on the following ''quasiequilibrium'' form $P_i^{qe}(t)$:

$$P_i(t) \approx P_i^{qe}(t) = \frac{g_i(t)}{Z} e^{E_i/T},$$

$$Z = \sum_{i=-\infty}^{\infty} g_i(t) e^{E_i/T}, \tag{11}$$

where the ''form factors'' $g_i(t)$ are slowly varying and decay on the scale of $\xi(t)$. (Note that the energy barrier $E_i>0$ is the opposite of the energy of the site.) This idea of ''partial equilibrium'' is actually quite general and is often advocated in the context of glassy dynamics. Although the system is out of equilibrium, one may think of its state at time t as of a partial equilibrium restricted to the region of phase space that it has explored up to time t, see, e.g., Refs. [36–38]. This idea of partial equilibrium was introduced and used quantitatively in the context of random walk models in Ref. [29].

In this section, we want to discuss this issue in some details. It turns out that the full statistics of P_i^{qe} can be worked out in the limit, where $\xi(t)\to\infty$, and can be compared to the corresponding statistics of $P_i(t)$ that we determine numerically. Perhaps surprisingly, we find that these statistics differ significantly even in the long-time limit, meaning that the out of equilibrium problem never approaches a quasiequilibrium regime.

A. Participation ratios and localization

In order to investigate the statistical property of a random probability measure [such as $P_i(t)$ or P_i^{qe}], one can introduce the following distribution:

$$\varphi(P) = \left\langle \sum_i P\,\delta(P-P_i) \right\rangle_\tau, \quad 0<P<1, \tag{12}$$

which is defined in such a way as to give a small weight to the very large number of sites with small energies, in order to evidence the statistics of the deeper traps present in the system. This distribution $\varphi(P)$ is normalized, since

$$\int_0^1 \varphi(P)\,dP = \left\langle \sum_i P_i \right\rangle_\tau = 1. \tag{13}$$

The moments of this distribution are related to the so-called inverse participation ratios Y_k:

$$\int_0^1 P^{k-1}\varphi(P)\,dP = \left\langle \sum_i P_i^k \right\rangle_\tau = Y_k. \tag{14}$$

These participation ratios have an interesting interpretation: if Y_k remains finite for $k>1$ as the number of terms in the sum diverges, one speaks of *localization*, since a finite fraction of the number of particles remain concentrated on a finite number of sites, even in the limit of an infinite number of available sites. The Y_k were introduced in the context of electronic localization [39] and in spin glass theory [40], and studied in several other problems [41,42]. Note that in the limit $k\to 1$, $(Y_k-1)/(1-k)$ becomes the statistical entropy of the measure P_i.

In equilibrium, and for integer values of k, Y_k can be interpreted as follows. Suppose one chooses at random k particles with their corresponding equilibrium weight, Y_k is the probability to find them all at the same site. Correspondingly, for the out of equilibrium situation, Y_k is the probability to find k particles (that all started at the same site) clustered together on the same site at time t. Obviously Y_k can only be nonzero if some effective attraction exists between the particles. In the case of disordered systems, this attraction is induced by the disordered environment, where (noninteracting) particles condense into particularly favorable sites.

For the problem at hand, the quasiequilibrium value Y_k^{qe} of the participation ratios can be computed, using for in-

stance auxiliary integrals [41] (see also Refs. [43,44]). Interestingly, the detailed shape of the "form factors" g_i in Eq. (11) does not matter, and the quasiequilibrium results Y_k^{qe} coincide with the equilibrium values Y_k^{eq}. For $\mu \geqslant 1$, Y_k^{eq} tends to 0 when $\xi(t)$ goes to ∞, whereas for $\mu < 1$ it converges for large $\xi(t)$ to a finite value,

$$Y_k^{eq} = \frac{\Gamma(k-\mu)}{\Gamma(k)\Gamma(1-\mu)}, \tag{15}$$

identical to that found in the random energy model. Note that $Y_k^{eq} \to 0$ when $\mu \to 1^-$, so that $Y_k^{eq}(\mu)$ is continuous at $\mu = 1$, and the participation ratios indeed converge to 0 in the critical case, although rather slowly. This means that in the low temperature phase $T < T_g$, the equilibrium measure localizes over a finite set of sites. The corresponding equilibrium distribution of weights is given by

$$\varphi_{eq}(P) = \frac{1}{\Gamma(1-\mu)\Gamma(\mu)} P^{-\mu}(1-P)^{\mu-1}. \tag{16}$$

In order to test the partial equilibrium idea, a relevant question is whether or not the dynamical $Y_k(t)$ approach, in the long-time limit, the equilibrium (infinite size) Y_k^{eq}. This can be also seen as a question about the commutation of the two limits $t \to \infty$ and $L \to \infty$ (see, e.g., Ref. [3]). The equilibrium case corresponds to taking $t \to \infty$ first, at fixed L, and then taking L to infinity. The out of equilibrium case, on the other hand, corresponds to taking $L = \infty$ from the outset and let $t \to \infty$.

B. Dynamical localization and weak ergodicity breaking

Let us now turn to the dynamical localization properties, starting from a localized initial condition, $P_i(t=0) = \delta_{i,0}$. It has been shown by Fontes, Isopi, and Newman [30] that the random walk process with a diverging local mean trapping time converges, up to a space-time rescaling, to a stationary process. Consequently, all spatially integrated (one-time) quantities like participation ratios converge to asymptotic values at large time, which are *a priori* different from the equilibrium ones. Unfortunately, this mathematical approach has not been yet able to predict the corresponding numerical values. We have computed numerically, using a simple Monte Carlo method, the time dependence of $Y_k(t)$ for several values of k ($k = 2, \frac{5}{2}, 3, \frac{7}{2}, 4$); see Appendix B for technical details. Our simulations confirm the convergence of $Y_k(t)$ towards a limiting value for large t, and show that these asymptotic values are indeed different from the equilibrium ones.

In order to evidence the convergence of $Y_k(t)$ towards different asymptotic values depending on the order of limits $t \to \infty$ and $L \to \infty$, we have first studied small systems for different sizes $L = 2N+1$, in the case $\mu = 0.5$. Figure 4 shows the onset of a clear plateau at a value $Y_2^{dyn}(L)$ smaller than the value predicted by Eq. (15), $Y_2^{eq} = 0.5$ (for $L \to \infty$), before a crossover towards the equilibrium regime. Rescaling the time coordinate by a factor $N^{(1+\mu)/\mu}$ (corresponding to the equilibration time t_{erg} of the system), the data collapse

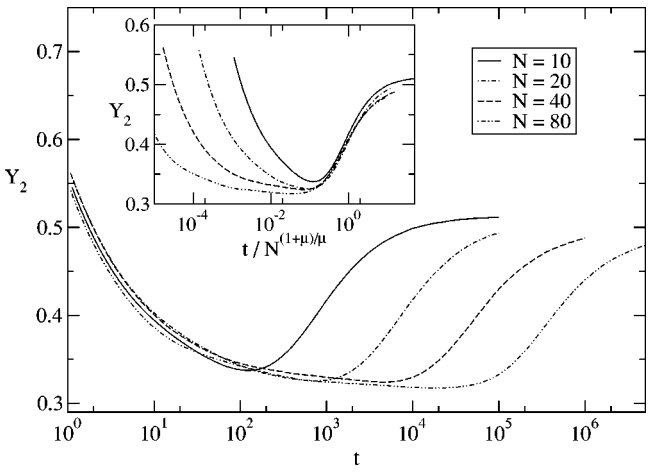

FIG. 4. Test of the convergence of $Y_2(t)$ towards an out of equilibrium value, for $\mu = 0.5$: $Y_2(t)$ is plotted for different small sizes $L = 2N+1$ of the system, so that equilibration can be reached within simulation time. One can see the onset of a plateau at a value lower that $Y_k^{eq} = 0.5$ (the equilibrium value for $L \to \infty$). The inset shows that the curves collapse if time is rescaled by the equilibration time $t_{erg} \propto N^{(1+\mu)/\mu}$, so that the plateau corresponds to a true out of equilibrium effect, and not to an initial transient.

rather well, at least in the crossover region. This shows that the plateau indeed corresponds to the onset of an out of equilibrium steady state regime, when the diffusion length is much smaller than the size of the system. The crossover appears when the two lengths become comparable.

In order to study the asymptotic value $Y_2^{dyn} \equiv Y_2^{dyn}(L \to \infty)$, we have simulated systems of very large sizes L. However, the temporal convergence of $Y_2(t)$ is very slow and some infinite-time extrapolation procedure is needed. As illustrated in the inset of Fig. 5 for $k = 2$ and $\mu = 0.5$, we have assumed a power-law convergence of Y_k, of the form $Y_k(t) = Y_k^{dyn} + At^{-a}$ with 3 fitting parameters Y_k^{dyn}, A and a, which was found to work rather well. However, for μ close to 1, the fitting parameter Y_k^{dyn} becomes very sensitive to the choice of the time interval used to fit the data, and as a result, error bars become larger.

Figure 5 shows the extrapolated Y_2^{dyn} and Y_3^{dyn} as a function of μ, and compares it to the equilibrium relation $Y_2^{eq}(\mu) = 1-\mu$, and $Y_3^{eq}(\mu) = (1-\mu)(1-\mu/2)$. It appears that the dynamical localization is weaker than in equilibrium. In particular, Y_2^{dyn} and Y_3^{dyn} converge to a value smaller than 1 when μ goes to 0. We shall argue below that $Y_k^{dyn}(\mu = 0) = 2/(k+1)$, whereas $Y_k^{eq}(\mu = 0) = 1$. In the other limit, $\mu \to 1$, it will also be argued in the following section that Y_k^{dyn} vanishes linearly with μ. This is indeed compatible with the numerical data, although other functional dependence might also be compatible, since the error bars are large in this range of μ. We have also shown in Fig. 5 the prediction of a simple argument given in Sec. IV D below, which suggests $Y_k^{dyn}(\mu) = 2Y_k^{eq}(\mu)/(k+1)$, which is in rather good agreement with the numerical results.

Therefore, all the dynamical participation ratios Y_k^{dyn} are different from their static counterpart. The relative weights of the different visited sites are not given by the ratio of their

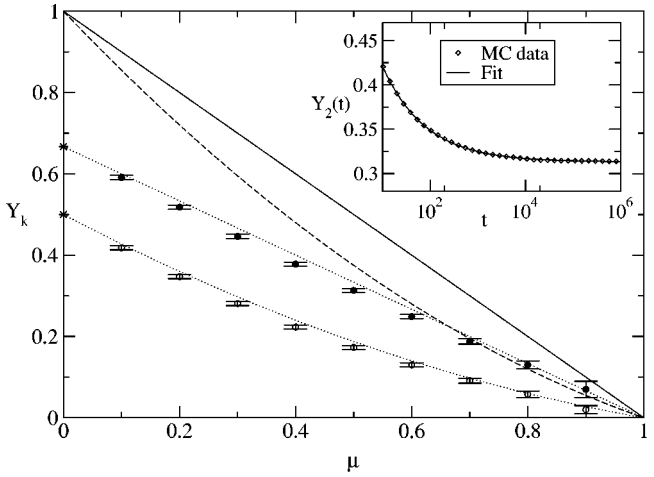

FIG. 5. Plot of Y_2^{dyn} (filled circles) and Y_3^{dyn} (empty circles) versus μ. The equilibrium functions $Y_2^{eq}(\mu)$ (full line) and $Y_3^{eq}(\mu)$ (dashed line) are shown for comparison. One clearly sees that localization is weaker than in the equilibrium situation. In particular, the participation ratios seem to converge to a zero temperature limit which is less than 1. The stars and the dotted lines correspond to the prediction of a simple model given below, Eq. (39). Inset: fit of $Y_2(t)$ using the functional form $Y_2(t)=Y_2^{dyn}+At^{-a}$, for $\mu=0.5$. Only 1 Monte Carlo point out of 12 is shown, for clarity.

Boltzmann weights. This result is important, since it was shown that, in the Sinai model, equilibrium and dynamical participation ratios indeed coincide [45]. An interesting possibility, discussed in the context of glassy systems, would be that the Y_k^{dyn} correspond to an equilibrium measure but at a different effective temperature. We will show below, that this is not the case.

Note that for walks in higher dimensions, $d>2$, one can show rigorously that $Y_k^{dyn}=0$ [31], whereas Y_k^{eq} are still given by Eq. (15).[1] However, in this case, each site is visited a finite number of times, and therefore it could have been expected that the idea of partial equilibrium over the set of visited sites would be quantitatively incorrect (although it is able to reproduce, at least qualitatively, some nontrivial dynamical correlation functions— [29] and see below). Another solvable case is the one-dimensional directed walk, where each site is visited once. In this case, Y_2^{dyn} can be computed exactly [33] and is found to be close to, but different from, the equilibrium value $1-\mu$.

The surprising aspect of our result in one dimension is that each site is visited, asymptotically, an infinite number of times—a feature that, at least naively, should lead to partial equilibration.

A different, but related, issue concerns the fraction $f_i(t)$ of the total time t a *given* particle has spent in the ith trap, and study the participation ratios of this quantity. In this case, we have found numerically that the different Y_k *are* given by the equilibrium formula, Eq. (15). Therefore, we are in a situation where ergodicity is (weakly) broken: the relative time a given particle spends on different sites has not the same statistics as the relative fraction of particles that are found on the different sites at a given instant of time. Such a difference between individual and ensemble measurements have been emphasized in a different context in Ref. [22], and recently observed experimentally [24].

[1]The case $d=2$ is marginal, but one still finds that $Y_k^{dyn}=0$ in that case [31].

C. Analytical calculation of the participation ratio

Using the same procedure as for $\langle p(x,t)\rangle_\tau$, one could try to compute $Y_k(t)$ that is given by

$$Y_k(t)=\int_{-\infty}^{\infty} dx\langle p(x,t)^k\rangle_\tau. \tag{17}$$

However, this calculation reveals to be much harder than for the case of $\langle p(x,t)\rangle_\tau$. In Appendix C, we report a simplified calculation in the case $k=2$, which aim is to argue that Y_2^{dyn} is different from 0 in the low temperature phase $\mu<1$, whereas it vanishes for $\mu>1$. Although this last result has been rigorously proven in Ref. [30], we want to introduce here a general method that could, in principle, yield bounds and approximations for Y_k for any μ, and not only for $\mu<1$. We obtain the behavior of Y_2^{dyn} for $\mu\to 1^-$ and find how $Y_2(t)$ vanishes as a function of t for $\mu>1$. To do this, we introduce a function $R(t,t')$ through

$$R(t,t')=\int_{-\infty}^{\infty} dx\langle p(x,t)p(x,t')\rangle_\tau \tag{18}$$

[so that $Y_2(t)=R(t,t)$], as well as its Laplace transform $\hat{R}(s,s')$,

$$\hat{R}(s,s')=\int_0^\infty dt\int_0^\infty dt'' e^{-st-s't'}R(t,t'). \tag{19}$$

Using rather crude approximations, we obtain that, in the particular case where $s=s'$ and $\mu<1$:

$$\hat{R}(s,s)\simeq\frac{R_0}{s^2},\quad s\to 0, \tag{20}$$

with a finite coefficient R_0. In order to interpret this result, we assume that $R(t,t')$ obeys, for large t,t', a scaling relation of the form

$$R(t,t')=Y_2^{dyn}\mathcal{R}\left(\frac{t}{t'}\right), \tag{21}$$

which we have confirmed using numerical simulations. Then one gets

$$\hat{R}(s,s)\sim\frac{2Y_2^{dyn}}{s^2}\int_1^\infty du\frac{\mathcal{R}(u)}{(1+u)^2}, \tag{22}$$

or, using Eq. (20),

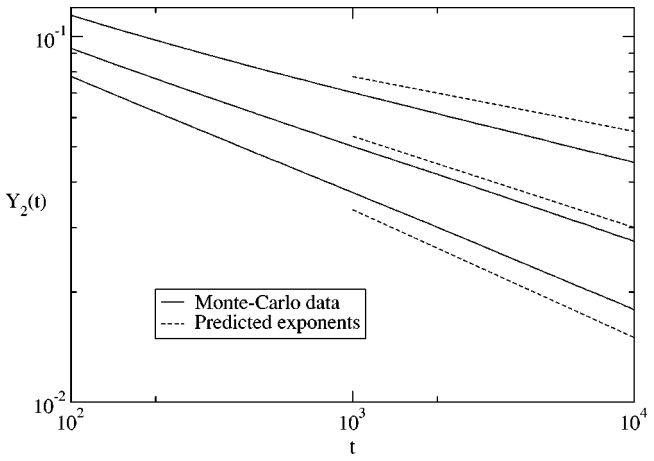

FIG. 6. Plot of $Y_2(t)$ for $\mu=1.3$, 1.5, and 1.7 (full lines, from top to bottom), showing a power-law decay compatible with the predicted behavior $t^{(1-\mu)/2}$ (dashed lines). Note that the subleading corrections become stronger when μ is close either to $\mu=1$ or to $\mu=2$.

$$Y_2^{dyn}=\frac{R_0}{2\int_1^\infty du\frac{\mathcal{R}(u)}{(1+u)^2}}. \tag{23}$$

Since the integral appearing in the above equation is convergent [because $\mathcal{R}(u)\leqslant 1$], this result suggests that Y_2^{dyn} is finite when $\mu<1$. Since we find that R_0 vanishes linearly when $\mu\to 1^-$, we conjecture that

$$Y_2^{dyn}\propto 1-\mu \quad (\mu\to 1), \tag{24}$$

which is compatible with the numerics and also comparable with the equilibrium behavior. The same level of approximation on Y_3 also leads to a finite limit Y_3^{dyn}, and to a linear temperature behavior $Y_3^{dyn}\propto 1-\mu$ $(\mu\to 1)$, so that one can reasonably guess that this linear dependence is valid for all $k>1$.

The case $\mu>1$ has also been studied; we find for $1<\mu<2$ the new predictions,

$$\hat{R}(s,s)\sim\frac{1}{(s^{5-\mu/2})} \quad (1<\mu<2)$$

$$\hat{R}(s,s)\sim\frac{1}{s^{3/2}} \quad (\mu>2), \tag{25}$$

which predicts that $Y_2(t)$ tends to zero as $t^{(1-\mu)/2}$ when $1<\mu<2$, and as $t^{-1/2}$ whenever $\mu>2$. The last result is indeed expected: when the second moment of $\psi(\tau)$ exists, diffusion is normal with no anomalous corrections. The probability that two particles starting at time 0 at the same site happen to be again on the same site at time t decays as $\xi(t)\times 1/\xi(t)^2\propto 1/\sqrt{t}$. The result for $1<\mu<2$ has been checked numerically for $\mu=1.3$, 1.5, and 1.7 (see Fig. 6).

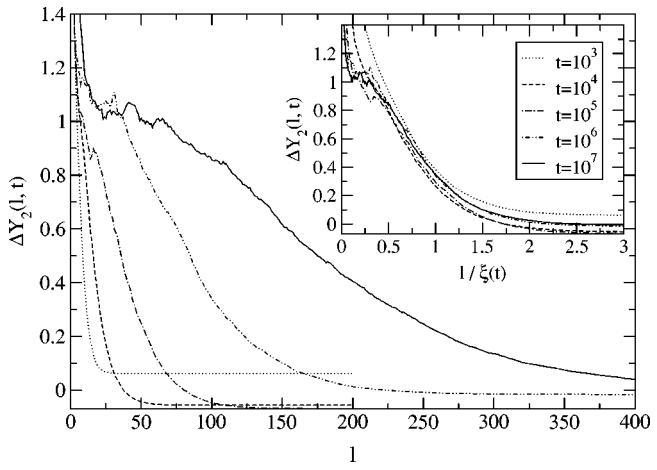

FIG. 7. Plot of $\Delta Y_2(\ell,t)$ versus ℓ for $\mu=0.5$ and $t=10^3$, 10^4, 10^5, 10^6, and 10^7, so that $\xi(t)$ ranges from 10 to 215. Inset: the size ℓ of the window is rescaled by $\xi(t)$, and the resulting collapse of the curves shows that the equilibration length scale is of the order of a fraction of $\xi(t)$. The strong increase of $\Delta Y_2(\ell,t)$ for small ℓ is due to small size effects.

D. Partial equilibrium in a finite region

We have seen that the dynamical participation ratio never reaches the static equilibrium value. Can one, however, isolate a region of space, of size $\ell(t)$ possibly much smaller than $\xi(t)$, such that inside that region equilibrium is reached ? In order to test this idea, one can define a spatially restricted participation ratio $Y_k(\ell,t)$ in the following way as

$$Y_k(\ell,t)=\sum_{|i|\leqslant\ell}\tilde{P}_i(t)^k, \tag{26}$$

where $\tilde{P}_i(t)$ is the probability that the walk is on site i conditioned to the fact that it is within the interval $[-\ell,\ell]$

$$\tilde{P}_i(t)=\frac{P_i(t)}{\sum_{|j|\leqslant\ell}P_j(t)}. \tag{27}$$

Figure 7 shows the numerical results for the following rescaled quantity:

$$\Delta Y_2(\ell,t)=\frac{Y_2(\ell,t)-Y_2^{dyn}}{Y_2^{eq}-Y_2^{dyn}}, \tag{28}$$

such that $\Delta Y_2=1$ for an equilibrated region, and 0 by construction for $\ell\gg\xi(t)$.

The results are obtained with t ranging from 10^3 to 10^7, and $\mu=0.5$. When t goes to ∞ at fixed ℓ, $Y_2(\ell,t)$ is seen to converge to the corresponding equilibrium value [which depends slightly on ℓ: Eq. (15) is only valid in the limit of large sizes]. In the inset we show $\Delta Y_2(\ell,t)$ as a function of $\ell/\xi(t)$. The collapse is rather good, showing that the size up to which the system is equilibrated grows as $\xi(t)$, which is thus the only dynamical length scale of this model. That $Y_2(\ell,t)$ is equal to the equilibrium value for $\ell<\phi\xi(t)$,

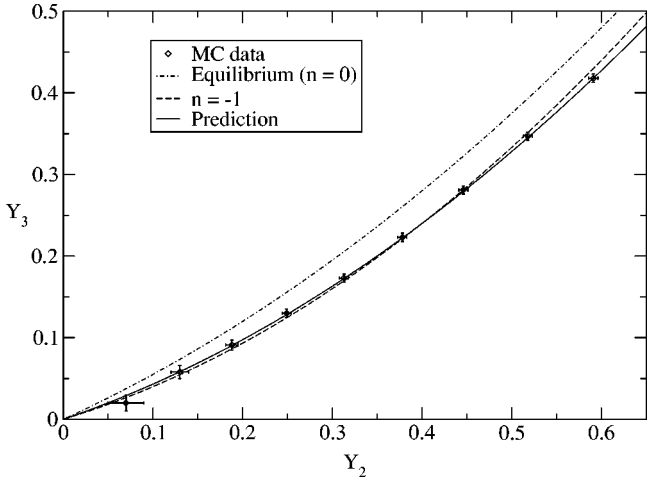

FIG. 8. Plot of $Y_3^{dyn}(\mu)$ versus $Y_2^{dyn}(\mu)$, parametrized by μ. The equilibrium relation, corresponding to $n=0$ in the replica language, is shown for comparison (dotted line). A rather good account of the data is obtained using $n=-1$ (dashed line). However, as we show below, a better description is obtained using a mixture of $n=-2$ cases, see Eq. (39) (full line).

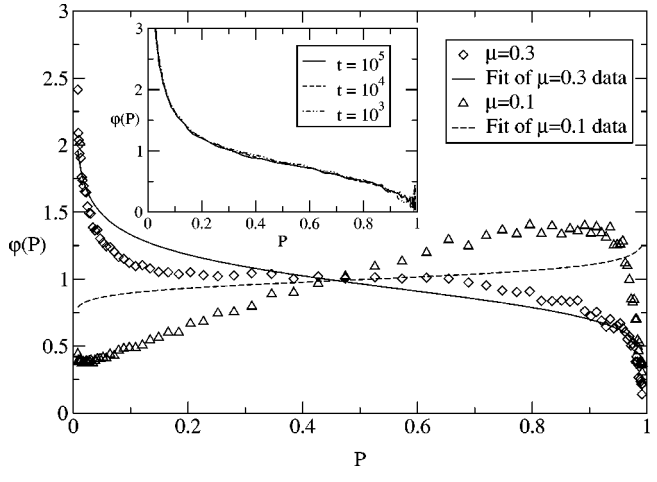

FIG. 9. Fit of $\varphi(P)$ with the $n=-1$ ansatz [Eq. (32)] using $\tilde{\mu}$ as a free parameter, for $\mu=0.3$ and $\mu=0.1$. The fit is worse and worse as μ is decreased. Note that for higher values of μ, the fits are better. Inset, $\varphi(P,t)$ is plotted for different times $t=10^3$ (full line), 10^4 (dashed line) and 10^5 (dotted line) in order to evidence the convergence towards an out of equilibrium distribution $\varphi_{dyn}(P)$ ($\mu=0.5$).

where ϕ is a small number, means that only the ''contemporary'' processes concerning the largest scale $\xi(t)$ are out of equilibrium. In the sense, this could have been expected. However, let us emphasize again that a simple description such as Eq. (11), which describes the lack of equilibrium on the scale of ξ through the form factors $g_i(t)$, cannot explain the observed difference between Y_2^{eq} and Y_2^{dyn}.

IV. GENERALIZED EQUILIBRIUM AND HALF SPACE EXCURSIONS

A. A functional relation between the Y_k's

We have seen that the dynamical participation ratios do not take their equilibrium value. Would it be possible to redefine an effective temperature $\tilde{\mu}$ such that all Y_k can be expressed as equilibrium values with this effective temperature? In order to test this idea, one can eliminate μ from the relation Eq. (15), and reexpress all Y_k as a function of Y_2, which yields the following relation:

$$Y_k = f_k(Y_2) = \frac{\Gamma(k-1+Y_2)}{\Gamma(k)\Gamma(Y_2)}. \tag{29}$$

In Fig. 8, we have plotted Y_3^{dyn} versus Y_2^{dyn} for several values of μ. It appears clearly that this relation is different from the equilibrium one, shown for comparison. This rules out the possibility of defining a meaningful temperature from Y_2^{dyn}.

The above relation between the Y_k is known to be incorrect in other models, such as in the random map, for example (see Ref. [41]). Inspired from the replica method, one can formally generalize Eq. (15) to

$$Y_{k,n} = \frac{\Gamma(1-n)\Gamma(k-\mu)}{\Gamma(k-n)\Gamma(1-\mu)}, \tag{30}$$

where n is the number of replicas (that must be set to $n=0$ to recover Eq. (15), see Refs. [41,44]). We can then express $Y_{k,n}$ as a function of $Y_{2,n}$ for arbitrary n. We found that the value $n=-1$ gives a reasonable account of the data for all μ values. Interestingly, this value $n=-1$ was found to describe exactly the ''area preserving random map model'' considered in Ref. [41] (where other models, corresponding to different negative values of n, where also studied). However, as we discuss now, a more precise investigation of the problem shows that $n=-1$ does not fully describe our results.

B. The dynamical distribution of weights

Instead of studying all the different Y_k's, one can analyze directly the time evolution of the distribution of weights, $\varphi(P,t)$, defined as [see also Eq. (12)]:

$$\varphi(P,t) = \left\langle \sum_i P\,\delta(P-P_i(t)) \right\rangle_\tau, \quad 0<P<1. \tag{31}$$

For long times in an infinite system, this distribution is expected to reach a stationary distribution $\varphi_{dyn}(P)$. The inset of Fig. 9 shows $\varphi(P,t)$ for three successive (large) times: $t=10^3$, 10^4, and 10^5. All three curves collapse rather well, at least not close to the ''edges'' $P=0$ and $P=1$, showing that we are close to the asymptotic distribution. (However, since the Y_k's are sensitive to the region around $P=1$, the discrepancies at the edges explain why these moments converge more slowly.)

One can define a generalized distribution $\varphi_{n,\tilde{\mu}}(P)$ as the one generating the $Y_{k,n}(\tilde{\mu})$, which leads to the following beta distribution:

$$\varphi_{n,\tilde{\mu}}(P) = \frac{\Gamma(1-n)}{\Gamma(1-\tilde{\mu})\Gamma(\tilde{\mu}-n)} P^{-\tilde{\mu}}(1-P)^{\tilde{\mu}-n-1}. \tag{32}$$

Following the same line of thought as in the preceding section, we want to check more precisely if the data are compatible with $n=-1$.

The parametric plot $Y_3^{dyn}(Y_2^{dyn})$ was just a convenient way to test whether Y_3^{dyn} and Y_2^{dyn} obey a relation of the type Eq. (30), with μ replaced by an unknown parameter $\tilde{\mu}$. Turning to $\varphi_{dyn}(P)$, one can then consider $\tilde{\mu}$ as a free parameter, and try to fit the numerical data, fixing n to the value $n=-1$ found in the preceding section. For $\mu \geqslant 0.5$ the fits obtained are correct (data not shown). On the contrary, for $\mu<0.5$ the best fits appear to be quite unsatisfactory, in particular, for $\mu=0.1$ (see Fig. 9), showing that the $n=-1$ ansatz does not fully account for the numerical data. This is due to the fact that $\varphi_{n,\tilde{\mu}}(P)$ is a monotonous function whatever the value of $\tilde{\mu}$, whereas $\varphi_{dyn}(P)$ becomes nonmonotonic for low values of μ, so that the former cannot fit correctly the latter. As a result, the numerical data cannot be described by a formula of the type of Eq. (32), in particular, in the very low temperature case, although this ansatz was rather correctly accounting for the parametric plot $Y_3^{dyn}(Y_2^{dyn})$. In order to get a better understanding of this dynamical localization phenomena, we shall now focus on the case $\mu \to 0$, where simple arguments can be proposed.

C. A simple analytical argument in the limit $\mu \to 0$

Although the out of equilibrium localization problem seems to be hard to tackle at finite temperature, a simple argument can be given in the limit $\mu \to 0$. This argument accounts for the nontrivial limits Y_2^{dyn} and Y_3^{dyn}, which were found to be less than 1 for $\mu \to 0$ (see Fig. 5). If μ is very small, then the largest trapping times accessible after a given time t are strongly separated from each other. One can, for example, show that the distribution of the ratio R of the second largest time over the largest is $p(R)=\mu R^{\mu-1}$, which tends to $\delta(R)$ when $\mu \to 0$. Therefore, in this limit, one can assume that the time elapsed before finding the deepest trap i_0 occupied at time t is negligible compared to the time spent in i_0.[2]

So the problem becomes equivalent to that of a random walk with no random potential, but with two absorbing boundaries (i.e., the traps with trapping time $>t$ to the right and to the left of the initial site) at random positions. If these absorbing sites are at distances, respectively, x_r and x_l from the initial position of the walk, then the probability to be absorbed by (say) the left boundary is $p_l=x_r/(x_l+x_r)$. Since the initial site can be anywhere between these two sites with equal probability, one finds that p_l is a random variable uniformly distributed over $[0,1]$. Coming back to the trap model, it means that only two sites can be occupied, and the corresponding occupation rates are uniform random variables. More precisely $\varphi(P)$ can be written as

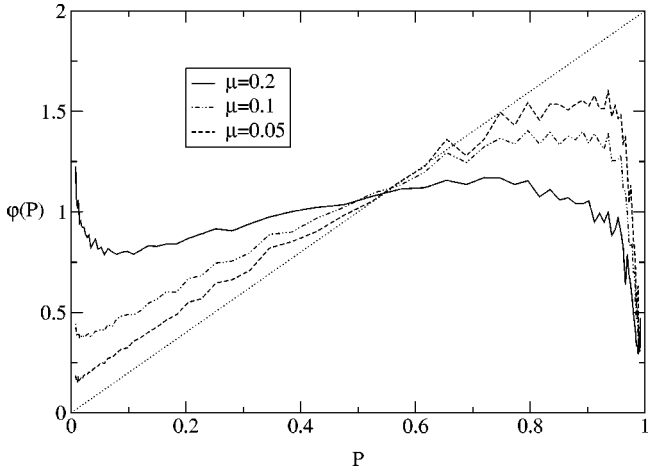

FIG. 10. $\varphi(P)$ for several small values of μ: $\mu=0.2$ (full line), 0.1 (dot-dashed line) and 0.05 (dashed line). The curves seem to converge towards the asymptotic distribution $\varphi_0(P)$ (dotted line) for $\mu \to 0$, but the convergence looks quite slow. Note that $P=0$ and $P=1$ are presumably singular points in this convergence process.

$$\varphi_0(P)=P\int_0^1 dp_l[\,\delta(p_l-P)+\delta(1-p_l-P)\,]=2P, \tag{33}$$

which leads for Y_k to

$$Y_k^0=\int_0^1 P^{k-1}\varphi_0(P)dP=\frac{2}{k+1}. \tag{34}$$

For the particular cases $k=2$ and $k=3$ presented above, this gives $Y_2^0=\frac{2}{3}$ and $Y_3^0=\frac{1}{2}$, which agrees rather well with what can be extrapolated from the numerical data on Fig. 5. Moreover, Fig. 10 confirms that $\varphi(P)$ converges towards $\varphi_0(P)$ when $\mu \to 0$, although rather slowly. Note also that $\varphi_0(P)$ can be written in the general form Eq. (32) given in the preceding section, for the special choice $n=-2$ and $\tilde{\mu}=-1$.

D. Generalization of the argument to finite temperature

The above argument can be reinterpreted in the following way. In equilibrium, the zero temperature limit means that a single site dominates and contains all the probability weight. This is why $Y_k^{eq} \to 1$ when $\mu \to 0$. On the other hand, in one dimension, the time needed to explore an interval of size L is $L^{(1+\mu)/\mu}$, which grows much faster than the time to exit the deepest traps ($\sim L^{1/\mu}$) found in the interval. Therefore, if a deep trap is encountered in say the left region of the line, there is a substantial probability that the particle will not have time to explore the right region and equilibrate with a trap of comparable depth. This is the essence of the above argument: at zero temperature, the fraction p_l of the weight captured by the left trap is uniform between zero and one, independently of the relative depth of the two traps. A simple way to generalize this argument for finite temperature is to assume that each half space is independently equilibrated,

[2]The time spent on site i_0 is actually much greater than the trapping time τ_{i_0}, since the particle comes back to it a large number of times before finding a deeper trap (see Sec. V).

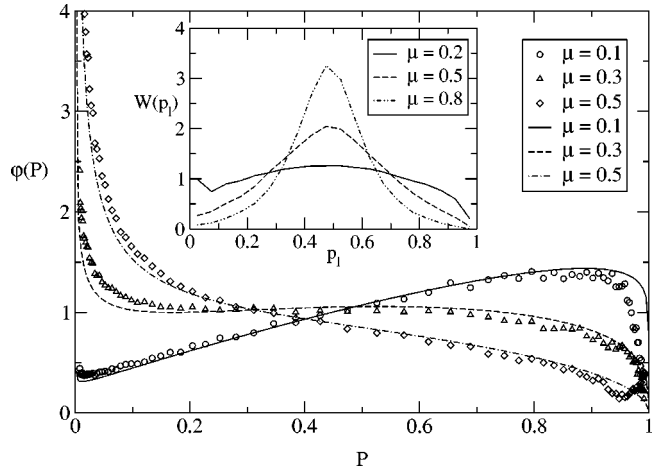

FIG. 11. Comparison between $\varphi(P)$ obtained by numerical simulations (symbols) and $\varphi^*(P)$ given by the argument developed in the text (lines). The agreement appears to be quite good, bearing in mind that no free parameter is used. Inset: distribution $W(p_l)$ of the probability weight p_l carried by one half space, for different μ. This distribution appears to be nonuniform (except for $\mu \to 0$), at variance with the hypothesis underlying Eq. (36).

and carries a total weight uniformly distributed between zero and one, as in the zero temperature limit. [Actually, as noticed above, we only need to assume that in each half space the probability distribution has the form given by Eq. (11) with arbitrary factors g_i: this does not affect the asymptotic shape of $\varphi(P)=\varphi_{eq}(P)$.] Denoting by $\varphi(P,p_l)$ the distribution restricted to the left half space, normalized to p_l, one has for $0<P<p_l$,

$$\varphi(P,p_l)=\frac{p_l}{\Gamma(1-\mu)\Gamma(\mu)}P^{-\mu}(p_l-P)^{\mu-1}. \tag{35}$$

Averaging over p_l with a uniform weight, and taking into account the right half space, leads to the following prediction for $\varphi(P)$,

$$\varphi(P)\simeq\varphi^*(P)=2\int_0^1 dp_l\varphi(P,p_l)\theta(p_l-P), \tag{36}$$

$$\varphi^*(P)=\frac{2}{\Gamma(1-\mu)\Gamma(1+\mu)}P^{1-\mu}(1-P)^{\mu} + \frac{2\mu}{\Gamma(1-\mu)\Gamma(2+\mu)}P^{-\mu}(1-P)^{1+\mu}. \tag{37}$$

Although we do not have any interpretation for this, one can notice that φ^* can be written as a superposition of distributions $\varphi_{-2,\tilde{\mu}}$, with two different values of $\tilde{\mu}$,

$$\varphi^*(P)=(1-\mu)\varphi_{-2,\mu-1}(P)+\mu\varphi_{-2,\mu}(P), \tag{38}$$

with $\varphi_{n,\tilde{\mu}}$ defined in Eq. (32), and in agreement with what was found for $\mu\to 0$. This prediction is compared with the numerics in Fig. 11, for several values of μ ($\mu=0.1$, 0.3, 0.5). The agreement is rather good; note that no fitting parameter is used here. We note that the participation ratios Y_k obtained using $\varphi^*(P)$ are simply proportional to the equilibrium values

$$Y_k^*=\frac{2}{k+1}Y_k^{eq}. \tag{39}$$

As shown in Fig. 5, this relation accounts quite well (but not exactly) for the data. However, the distribution $W(p_l)$ of the weight $p_l=1-p_r$ carried by one half space is not found to be uniform as we assumed, except for $\mu\to 0$—see the inset of Fig. 11. Surprisingly, if one redo the above computation with a humped shaped distribution $W(p_l)=A[p_l(1-p_l)]^{\sigma}$, the resulting $\varphi^*(P)$ does not fit the data as well as the above form, which corresponds to $\sigma=0$.

E. Discussion

The physical picture emerging from the last sections is the following. For the purpose of understanding global localization quantities, one can reasonably consider that space is split into two half lines, and that each one behaves as if it was independently equilibrated, but out of equilibrium with respect to the other. On the other hand, we have seen in Sec. III D that length scales much smaller than ξ could be considered as equilibrated, and that departure from equilibrium comes from the largest length scale $|x|\gtrsim\xi$. The equilibration of the small scales cannot be accounted for by the previous argument. All these observations suggest, in order to get a consistent picture, that space may be actually divided into three regions, an equilibrated domain centered on the origin and two quasiequilibrated regions on each side, and that each part of space is not equilibrated with the others.

An artificial remedy to this lack of equilibration between the different regions is to allow the particle to make long jumps. We have therefore added links between the sites x and $-x$, such that the probability to hop directly from x and $-x$ decays as $x^{-\rho}$. When ρ is large enough, the dynamical participation ratio $Y_2(t)$ is a decreasing function of time, and seems to converge to Y_2^{dyn}. When $\rho<\rho_c$ on the other hand, $Y_2(t)$ is seen to reach a minimum and to increase back towards the equilibrium value Y_2^{eq}. We have, however, not checked in details whether $Y_2(t)$ indeed converges towards Y_2^{eq} for all $\rho<\rho_c$, but only wanted to illustrate that the difference between Y_2^{dyn} and Y_2^{eq} is due to the scarcity of the links between the different sites for the one-dimensional lattice.

V. CORRELATION FUNCTIONS, AGING AND SUBAGING

A. Motivation

Let us now turn to different correlation functions that one can define in order to probe the peculiar *aging* properties of this model. Since the largest encountered trapping time during t_w scales as t_w^{ν} with $\nu=1/1+\mu<1$, one would naively expect that two-time correlation functions vary on a time scale $\sim t_w^{\nu}$. This would correspond to "subaging" behavior, where the effective relaxation time grows less rapidly than t_w itself.

This is indeed the case for the probability $\Pi(t_w+t,t_w)$ of not having jumped at all between times t_w and t_w+t. This correlation function was computed numerically in Ref. [29], and was found to scale very accurately as $\Pi(t_w+t,t_w) = \pi(t/t_w^\nu)$. The shape of the scaling function was compared to the prediction of an approximate calculation where one assumes ''partial equilibrium,'' i.e., that the probability to find the particle in a trap of depth τ after time t_w is equal to the equilibrium probability within a region of size $\xi(t_w)$. This approximation predicts a power-law behavior for $\pi(s)$ both for small and large s, with exponents that agree with their numerical determination. The detailed shape of $\pi(s)$, however, departs from the numerical results, which is expected. The success of the partial equilibrium assumption here is due to the fact that $\Pi(t_w+t,t_w)$ only depends on the average probability to occupy a site, and not on higher order correlations such as needed to compute the participation ratios Y_k.

Perhaps surprisingly, different correlation functions may exhibit a completely different aging behavior. Consider the probability $C(t_w+t,t_w)$ that the particle occupies the same site at time t_w+t and at time t. Obviously, $C(t_w+t,t_w) \geqslant \Pi(t_w+t,t_w)$. But in this case, it was shown rigorously in Refs. [30,31] that $C(t_w+t,t_w)$ scales as a function of t/t_w, and *not* as t/t_w^ν. This means that even if the particle has almost certainly jumped away from its starting point after a time $t_w^\nu \ll t_w$, it has returned there even after a time of order t_w so as to make $C(2t_w,t_w)=O(1)$, whereas $\Pi(2t_w,t_w) \to 0$. This difference is not intuitive *a priori*, in particular because one knows that once the particle has left its initial trap after a time $\sim t_w^\nu$, it takes on average an infinite time to get back there, since the walk is one dimensional. But if $C(t_w+t,t_w)$ is to decay on the scale t_w, it means that the probability not to find the particle on its starting point after a time t much greater than t_w^ν, but much less than t_w must tend to zero when $t_w \to \infty$. The fact that the particle jumps back and forth a large number of times between t_w^ν and t_w could thus *a priori* lead to an interesting behavior of $C(t_w+t,t_w)$ in the short-time regime $t/t_w \ll 1$ (which was not investigated in [30]). For example, one could find, as in Ref. [29], different ''time domains'' $t \sim t_w^{\nu_1}$, $t \sim t_w^{\nu_2}$, etc., where the correlation function has a different analytic behavior. This is the issue that we discuss below.

B. Analytical arguments

The difference of scaling between Π and C can be qualitatively understood as follows. For $C(t_w+t,t_w)$ to decay to zero, one has to wait until the region probed by the particle at time t_w+t is much larger than the initial region where it was located, i.e., a time t such that $\xi(t_w+t) \gg \xi(t_w)$. But since $\xi(t_w) \sim t_w^{\mu/(1+\mu)}$, the time needed for C to decay to zero is necessarily of order t_w. [Note that this argument does not hold for $\Pi(t_w+t,t_w)$, which only requires the particle to hop once out of its initial trap.]

In the same spirit as Ref. [29] for $\Pi(t_w+t,t_w)$, but using a slightly different method, one can try to give an approximate calculation of $C(t_w+t,t_w)$. The first step is to introduce the dynamical distribution of trapping times $p(\tau,t_w)$, assumed to behave as

$$p(\tau,t_w) \simeq \frac{1}{t_w^\nu}\phi\left(\frac{\tau}{t_w^\nu}\right). \tag{40}$$

This encodes the fact that typical trapping times are of order t_w^ν. If one assumes that short-time scales ($\tau \ll t_w^\nu$) are equilibrated, whereas large ones ($\tau \gg t_w^\nu$) are still distributed according to the *a priori* distribution (this can be rigorously proved in the fully connected trap model), one obtains the following asymptotic behavior for $\phi(z)$:

$$\phi(z) \simeq \frac{\gamma_0}{z^\mu}, \quad z \to 0, \tag{41}$$

$$\phi(z) \simeq \frac{\gamma_\infty}{z^{1+\mu}}, \quad z \to +\infty. \tag{42}$$

Using the relation

$$\Pi(t_w+t,t_w) = \int_1^\infty d\tau p(\tau,t_w) e^{-t/\tau}, \tag{43}$$

one can easily deduce from Eq. (41) the short-and late-time behavior of $\Pi(t_w+t,t_w)$,

$$\Pi(t_w+t,t_w) \simeq 1 - \frac{\gamma_0}{1-\mu}\Gamma(\mu)\left(\frac{t}{t_w^\nu}\right)^{1-\mu}, \quad t \ll t_w^\nu, \tag{44}$$

$$\Pi(t_w+t,t_w) \simeq \gamma_\infty \Gamma(\mu)\left(\frac{t}{t_w^\nu}\right)^{-\mu}, \quad t \gg t_w^\nu, \tag{45}$$

in agreement with the results of Ref. [29], and with the numerics (see below).

Turning now to $C(t_w+t,t_w)$, one has to take into account the fact that when a particle leaves its trap, it will come back a large number of times before really escaping. We thus propose the following approximation. A particle will be considered to have truly left its initial trap if it has encountered a deeper trap during its excursion out of the original trap. Given a trapping time τ, the probability that $\tau' > \tau$ is given by

$$P(\tau' > \tau) = \int_\tau^\infty \frac{\mu d\tau'}{\tau'^{1+\mu}} = \frac{1}{\tau^\mu}. \tag{46}$$

So the probability $\tilde{p}(\ell,\tau)$ that the first trap encountered with a trapping time larger than τ is found at a distance ℓ is

$$\tilde{p}(\ell,\tau) = P(\tau' > \tau)[P(\tau' < \tau)]^{\ell-1} = \frac{1}{\tau^\mu}\left(1 - \frac{1}{\tau^\mu}\right)^{\ell-1}. \tag{47}$$

For large τ's, one has

$$\tilde{p}(\ell,\tau)\approx\frac{1}{\tau^{\mu}}e^{-\ell/\tau^{\mu}}. \tag{48}$$

Note that we only give here a scaling argument, and that corrections coming from the fact that there is a deeper trap on both sides are neglected. Conditioned to the fact that the deeper trap is situated at a distance ℓ, the particle has a probability $1/\ell$ to reach it, once it has jumped out of its initial trap. Therefore, the escape rate can be written as

$$w(\tau,\ell)=\frac{1}{\tau\ell}. \tag{49}$$

The correlation function $C(t_w+t,t_w)$ is then given by

$$C(t_w+t,t_w)\approx\int_1^{\infty}d\tau p(\tau,t_w)\int_1^{\infty}d\ell\tilde{p}(\ell,\tau)e^{-w(\tau,\ell)t}. \tag{50}$$

After a few changes of variables, and using the scaling relations of Eq. (41), one finds the following short-time and late-time behavior for $C(t_w+t,t_w)$,

$$C(t_w+t,t_w)\simeq 1-c_s\left(\frac{t}{t_w}\right)^{(1-\mu)/(1+\mu)}, \quad t\ll t_w, \tag{51}$$

$$C(t_w+t,t_w)\simeq c_l\left(\frac{t}{t_w}\right)^{-\mu/(1+\mu)}, \quad t\gg t_w, \tag{52}$$

where the constants c_s and c_l are given by

$$c_s=\frac{\gamma_0}{1-\mu}\Gamma\left(\frac{2\mu}{1+\mu}\right)^2, \tag{53}$$

$$c_l=\frac{\mu\gamma_{\infty}}{(1+\mu)^2}\Gamma\left(\frac{\mu}{1+\mu}\right)^2. \tag{54}$$

These values for the short-time and late-time singularity exponents, have, to our knowledge, not been reported before, although they should, in principle, be contained in the analysis of Ref. [30]. We now turn to a numerical investigation of these asymptotic predictions.

C. Numerical results and multiple time scales

Figure 12 displays $1-\Pi(t_w+t,t_w)$ as a function of $t/t_w^{1/(1+\mu)}$, and $C(t_w+t,t_w)$ as a function of t/t_w, for different waiting times ($t_w=10^3$, 10^4, 10^5, and 10^6) and at temperature $\mu=\frac{1}{2}$. The collapse is very satisfactory, confirming the validity of the predicted scaling relations.

Let us analyze in more details the short-time behavior of these correlation functions. When plotting $\ln(1-\Pi)$ as a function of $\ln(t/t_w^{\nu})$, the scaling is still quite well obeyed and in good agreement with the theoretical prediction $1-\Pi\sim(t/t_w^{\nu})^{1-\mu}$, obtained in Ref. [29], up to small-time corrections that vanish only when $\Gamma_0 t\gg 1$.

On the other hand, a similar plot of $\ln(1-C)$ as a function of $\ln(t/t_w)$ is less convincing, which could be the sign of

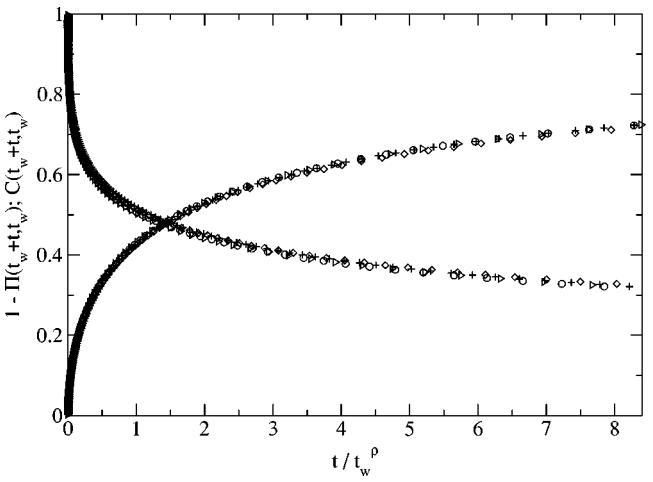

FIG. 12. Plot of $1-\Pi(t_w+t,t_w)$ (increasing curve) versus t/t_w^{ν} ($\rho=\nu$) and $C(t_w+t,t_w)$ (decreasing curve) versus t/t_w ($\rho=1$), for $\mu=\frac{1}{2}$, and $\nu=1/(1+\mu)=\frac{2}{3}$. The scaling relations are very well satisfied, at least in this time window. Symbols refer to the same waiting times for the two curves: $t_w=10^3$ (+), 10^4 ($\diamond$), 10^5 ($\circ$), and 10^6 ($\triangleright$).

multiple time regimes (as was the case in Ref. [29], where similar "nonscaling" features actually suggested such regimes). A way to investigate this issue is to study the function $g(\alpha,t_w)$ defined as

$$g(\alpha,t_w)=-\frac{\ln[1-C(t_w+t_w^{\alpha},t_w)]}{\ln t_w}. \tag{55}$$

If this function has a limit $g_{\infty}(\alpha)$ when $t_w\to\infty$, it means that in the time domain, where $t\sim t_w^{\alpha}$, the probability $1-C$ that the particle has escaped from its starting site decays as $t_w^{-g_{\infty}(\alpha)}$ for large t_w. From the t/t_w regime established by Ref. [30], we already know that $g_{\infty}(1)=0$. If $1-C(t_w+t,t_w)$ behaves as $(t/t_w)^{\lambda}$ even for $t\sim t_w^{\alpha}$ with $\alpha<1$, then one should observe $g_{\infty}(\alpha)=\lambda(1-\alpha)$. Any departure from a linear function $g_{\infty}(\alpha)$ would signal multiple time regimes; in particular, for the model considered in Ref. [29] in $d=1$ where two subaging exponents $\nu_2<\nu_1<1$ appear, one finds that the function $g_{\infty}(\alpha)$ is piecewise linear in the intervals $[0,\nu_2]$ and $[\nu_2,\nu_1]$, with different slopes. One also finds that $g_{\infty}(\nu_2^-)=g_{\infty}(\nu_2^+)$, and $g_{\infty}(\alpha>\nu_1)=0$. In this case, the change of slope indicates the presence of a characteristic time scale. One could imagine more complicated "multiscaling" situations, where $g_{\infty}(\alpha)$ is a nontrivial curve.

We have first tested this procedure on $\Pi(t_w+t,t_w)$, defining in the same way a function $g^*(\alpha,t_w)$ associated with Π. In this case, a single subaging scaling is expected, with $\nu=1/(1+\mu)$, and $\lambda=1-\mu$, which leads to $g_{\infty}(\alpha)=(1-\mu)(\nu-\alpha)$. The function $g^*(\alpha,t_w)$ is plotted for different values of t_w (namely, $t_w=10^4$, 10^5, 10^6, and 10^7) in Fig. 13, for $\mu=\frac{1}{2}$. On general grounds, one expects finite-time corrections to $g_{\infty}^*(\alpha)$ that decays as $1/\ln t_w$ and $1/t_w^{\gamma}$. Using these corrections, one can very satisfactorily extrapolate $g_{\infty}^*(\alpha,t_w)$ to a function which is very close to the expected

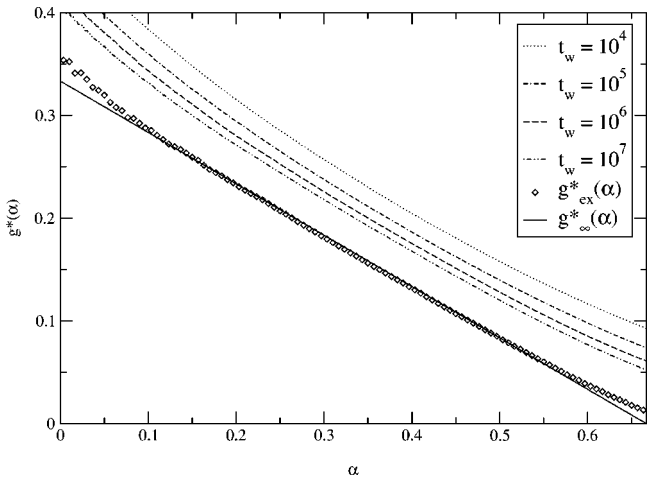

FIG. 13. Function $g^*(\alpha,t_w)$, associated to $\Pi(t_w+t,t_w)$, with $\mu=\frac{1}{2}$ and $t_w=10^4$, 10^5, 10^6, and 10^7. The function $g^*_\infty(\alpha)$ (full line) is expected to be $g^*_\infty(\alpha)=\frac{1}{2}(\frac{2}{3}-\alpha)$ (see text). The infinite-time extrapolation $g^*(\alpha,t_w)$ ($\diamond$) agrees very well with the prediction, with small discrepancies near $\alpha=0$ and $\alpha=\frac{2}{3}$, where finite-time effects are stronger.

result $g^*_\infty(\alpha)=\frac{1}{2}(\frac{2}{3}-\alpha)$ (see Fig. 13). To be more specific, we used the following functional form for the extrapolation:

$$g^*(\alpha,t_w)=g^*_\infty(\alpha)+\frac{b}{\ln t_w}+c(\alpha)t^{-\gamma(\alpha)}, \qquad (56)$$

where $g^*_\infty(\alpha)$, $c(\alpha)$, and $\gamma(\alpha)$ are fitted for each value of α, and b is a fitting coefficient independent of α, since the $1/\ln t_w$ correction is expected to come from the prefactor of $(t/t_w^\nu)^{1-\mu}$ in the short-time expansion of the correlation function. Therefore, the value of b was fixed from the direct power-law fit of the short-time regime of $1-\Pi$.

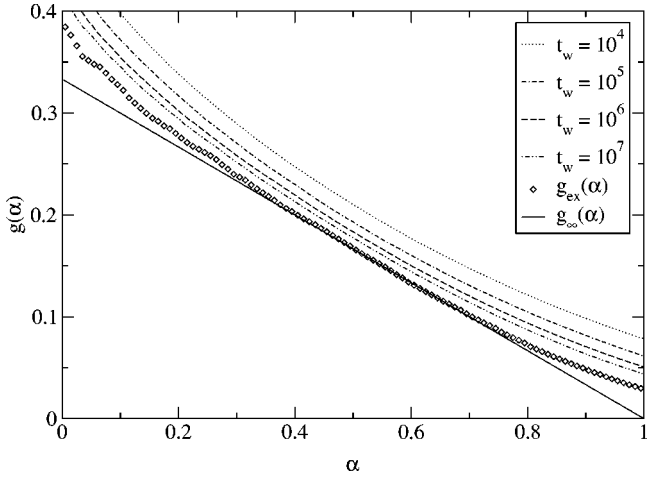

FIG. 14. Function $g(\alpha,t_w)$, associated with $C(t_w+t,t_w)$, for $\mu=\frac{1}{2}$ and with the same waiting times as for $g^*(\alpha,t_w)$. The argument developed in the text [Eq. (51)] predicts $g_\infty(\alpha)=\frac{1}{3}(1-\alpha)$ (full line). Although finite-time corrections are stronger than in the previous case, the infinite-time extrapolation $g_{ex}(\alpha)$ ($\diamond$) agrees well with the prediction, at least for $0.2<\alpha<0.8$.

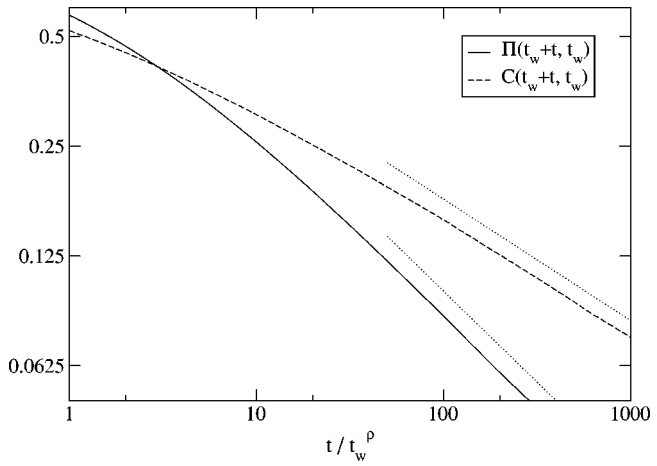

FIG. 15. Plot of the late time behavior of $\Pi(t_w+t,t_w)$ versus t/t_w^ν, and $C(t_w+t,t_w)$ versus t/t_w, for $t_w=10^5$ and 10^3, respectively, and $\mu=0.5$. Both correlation functions exhibit a power-law behavior at large time, and the exponents agree well with the predicted values $-\frac{1}{2}$ and $-\frac{1}{3}$ [see Eqs. (44) and (51)]. The corresponding slopes are shown in dotted lines, as a guide to the eye.

One can now apply the same procedure to $C(t_w+t,t_w)$. The results are shown in Fig. 14, using the same convention as for Fig. 13; $g(\alpha,t_w)$ is represented for the same waiting times as $g^*(\alpha,t_w)$. Interestingly, although finite-time corrections are strong, the extrapolated results are in good agreement with our analytical prediction $g_\infty(\alpha)=\lambda(1-\alpha)$, with $\lambda=(1-\mu)/(1+\mu)=1/3$, at least when $\alpha\in[0.2,0.8]$. This suggests that a unique time regime $t\sim t_w$ is relevant for $C(t_w+t,t_w)$, although we know that the time scale $t_w^\nu\ll t_w$ governs the evolution of Π. Note that the $1/\ln t_w$ corrections are weaker than in the previous case, and one is almost dominated by power-law corrections. This is due to the fact that the prefactor of $(t/t_w)^\lambda$ in the short-time regime happens to be close to 1 here (and hence the parameter b is small), whereas the prefactor of $(t/t_w^\nu)^\lambda$ was about 0.57 for Π.

So, what happens to the particles that have left the initial trap after a short-time t_w^ν and took a very long time to come back? The probability that a particle leaves the trap exactly at t' is $\partial[1-\Pi(t_w,t_w+t')]/\partial t'\sim t'^{-\mu}/t_w^{\nu(1-\mu)}$. If the sample was not disordered, the probability that it has not returned to the origin after time $t-t'$ decays as $(t-t')^{-1/2}$. Because of the long trapping times, this probability actually decays slower, as $(t-t')^{-\mu/(1+\mu)}$. These particles contribute to $1-C$, as

$$1-C(t_w+t,t_w)\sim\int_0^t dt'\frac{t'^{-\mu}}{t_w^{\nu(1-\mu)}}(t-t')^{-\mu/(1+\mu)}. \qquad (57)$$

Choosing $t=t_w^\alpha$, we find that the contribution of these ''early birds'' to $1-C$ is a factor of $t_w^{-\alpha\mu^2/(1+\mu)}$ smaller than the contribution computed above, Eq. (51), and are thus negligible in the large t_w limit.

This simple estimate shows (i) why finite-time corrections become large when $\alpha\to 0$, (ii) that power-law corrections to

$g(\alpha,t_w)$, as the one used for our extrapolation, are indeed expected and finally (iii) justifies why the t_w^ν time scale does not appear in $C(t_w+t,t_w)$.

The late time behavior of the two correlation functions can also be tested numerically. Fig. 15 shows $\Pi(t_w+t,t_w)$ versus t/t_w^ν, and $C(t_w+t,t_w)$ versus t/t_w, for $t_w=10^5$ and 10^3, respectively, and $\mu=0.5$. The two correlation functions behave as power laws at large time t, and the exponents are in good agreement with those predicted by Eqs. (44) and (51), shown for comparison (with a arbitrary prefactor), at least for this particular value of μ. Note that since we do not know the constants γ_0 and γ_∞, we cannot test the values predicted for the prefactors.

Finally, an important point to mention is whether or not this multiscaling behavior could be tested on mesurable quantities, in particular in a real system. Indeed, it would be interesting to know if response functions could be associated, in an unambiguous manner, to each of the correlation functions C and Π, and in such a case, if responses and correlations would scale in the same way with t and t_w. Several response functions could be proposed. One can, for instance, compute average probability current at time t_w+t, given that a small bias in the probability to go, say, to the right has been applied at time t_w. This response seems to have a well defined physical meaning; however, the way to relate it to the correlation C or Π is not obvious. Another definition of the response function, already introduced in the context of the fully connected trap model [13], is to associate to each site, in addition to the energy, a ''magnetization'' variable m_i. Assuming that m_i is independent from site to site and from the energy E_i, $C(t_w+t,t_w)$ appears to be the natural correlation of the magnetization

$$C(t_w+t,t_w)=\langle m(t_w)m(t_w+t)\rangle-\langle m(t_w)\rangle\langle m(t_w+t)\rangle, \tag{58}$$

where $m(t)$ is the magnetization of the system at time t, i.e., $m_{i(t)}$. But in this framework, the meaning of Π is not clear. Therefore, a careful study of this point is required, which will be done in a separate publication [46].

VI. CONCLUSION

In this paper, we have studied in details the one-dimensional exponential trap model, which exhibit a phase transition between a high temperature diffusive phase and a low temperature subdiffusive phase. We have obtained numerically and analytically the shape of the average diffusion front in the subdiffusive phase. Although based on an approximation valid only near the dynamical transition, our calculation provides several predictions on the asymptotic shape of $\langle p(x,t)\rangle$, which are in excellent agreement with the numerics. It would be interesting to see whether these predictions are actually exact.

The central result of this study concerns the localization properties. We have found that the dynamical participation ratios are all finite, but different from their equilibrium counterparts, even allowing for the existence of an effective, dynamical temperature. This is surprising because since each site is visited a very large number of times by the random walk, one could have expected that a partial equilibrium sets in within the limited region of space explored by the walk. Our detailed study of the distribution of dynamical weights shows that this is not the case. We have argued that this can be interpreted in terms of an effective ''fragmentation'' of space in two half lines (or even three domains), with a restricted equilibrium within each region, independently of the others.

Finally, we have studied two different two-time correlation functions, which exhibit different aging properties: one, $\Pi(t_w+t,t_w)$, is ''subaging'' whereas the other one, $C(t_w+t,t_w)$, shows ''full aging.'' We have given intuitive arguments and simple analytical approximations that account for these differences. We have obtained new predictions for the asymptotic (short-time and long-time) behavior of the scaling function associated to $C(t_w+t,t_w)$, which are found to be in excellent agreement with the numerics. Since two time scales (t_w^ν and t_w) appear in this model, one can wonder whether the short-time behavior of $C(t_w+t,t_w)$ exhibits a nontrivial, multiple time scaling. A careful numerical investigation of this issue leads to a negative answer, although strong finite time corrections are expected.

Since this one-dimensional model is currently of interest to the mathematical community, we hope that the study presented here will motivate further rigorous research, and that some of our results, in particular concerning asymptotic estimates, can be proven to be exact.

ACKNOWLEDGMENTS

Fruitful discussions on this model with G. Ben Arous, J.-M. Luck, C. Newman, P. Maass, M. Mézard, C. Monthus, and G. de Smedt are gratefully acknowledged.

APPENDIX A: THE AVERAGE DIFFUSION FRONT

1. Formulation of the problem

The explicit calculation of $\langle p(x,t)\rangle_\tau$ is reported is this Appendix. Note that all the computations developed in Appendix A and C are expected to be valid for the more general model where hopping is only constrained to have a finite range ℓ_{hop}, and in the long-time limit, i.e., when $\xi(t) \gg \ell_{hop}$. It is not necessary here to restrict ourselves to the nearest neighbor hopping case. Two different averages will be introduced, the average over the random walks $\langle\cdots\rangle_W$, and the average over the quenched trapping times $\langle\cdots\rangle_\tau$. We consider here a slightly modified version of the model, in which the particle stays on a site a time exactly equal to $\tau(x)$ (continuous notations are used, so as to facilitate the continuous space limit) rather than exponentially distributed around this value. We expect, and have checked numerically that this is irrelevant for the shape of $\langle p(x,t)\rangle_\tau$ at long times.

For a given sample of the disorder (quenched trapping times), we can decompose the probability $p(x,t)$ for the walker to be on site x at time t into a sum over the number n of steps

$$p(x,t)=\sum_{n=0}^{\infty} P(x,n;t)=\sum_{n=0}^{\infty} \langle \delta_{x_n,x} I(t_n<t<t_{n+1})\rangle_W, \tag{A1}$$

where $I(t_n<t<t_{n+1})$ is the characteristic function of the interval $[t_n,t_{n+1}]$, equal to 1 of t belongs to this interval, and 0 otherwise. In order to simplify the notations, we introduce $I_n(t)=I(t_n<t<t_{n+1})$. Now, averaging over the disorder,

$$\langle p(x,t)\rangle_\tau=\sum_{n=0}^{\infty} \langle\langle \delta_{x_n,x} I_n(t)\rangle_W\rangle_\tau. \tag{A2}$$

The key point is that we can permute the two averages, and perform first the average over the disorder for a given walk. Introducing the average $\langle\cdots\rangle_{n,x}$ over the n steps walks ending on site x, we get

$$\langle p(x,t)\rangle_\tau=\sum_{n=0}^{\infty} q(x|n)\langle\langle I_n(t)\rangle_\tau\rangle_{n,x}, \tag{A3}$$

where $q(x|n)$ is the standard probability for the random walk to be on site x after n steps

$$q(x|n)=\frac{1}{\sqrt{2\pi n}} e^{-x^2/2n} \tag{A4}$$

for large n. Taking the temporal Laplace transform $\mathcal{L}$ of $\langle p(x,t)\rangle_\tau$,

$$\langle \hat{p}(x,s)\rangle_\tau=\sum_{n=0}^{\infty} q(x|n)\langle\langle \hat{I}_n(s)\rangle_\tau\rangle_{n,x}, \tag{A5}$$

which requires the calculation of $\hat{I}_n(s)$,

$$\hat{I}_n(s)=\int_{t_n}^{t_{n+1}} e^{-st}dt=\frac{1}{s}e^{-st_n}[1-e^{-s(t_{n+1}-t_n)}]$$

$$\hat{I}_n(s)\simeq \tau(x)e^{-st_n}, \tag{A6}$$

since $t_{n+1}-t_n=\tau(x)$, and $\tau(x)$ is at most of order $s^{-\nu}$ when $s\to 0$, so that $s\tau(x)$ should be small. For a given walk W ending on site x after n steps, the time t_n can be decomposed into a sum over the different visited sites,

$$t_n=\sum_{x'} \mathcal{N}_W(x')\tau(x'), \tag{A7}$$

where $\mathcal{N}_W(x')$ is the number of visits of the site x' by the walk W. Now $\hat{I}_n(s)$ can be averaged over the disorder

$$\langle \hat{I}_n(s)\rangle_\tau=\langle \tau e^{-s\mathcal{N}_W(x)\tau}\rangle_\tau \prod_{x'\neq x} \langle e^{-s\mathcal{N}_W(x')\tau}\rangle_\tau. \tag{A8}$$

Averages of the form $\langle e^{-a\tau}\rangle_\tau$ or $\langle \tau e^{-a\tau}\rangle_\tau$ are easily calculated, in the limit $a\to 0$,

$$\langle e^{-a\tau}\rangle_\tau=\int_1^\infty \frac{\mu d\tau}{\tau^{1+\mu}} e^{-a\tau}\simeq 1-ca^\mu\simeq e^{-ca^\mu}, \tag{A9}$$

$$\langle \tau e^{-a\tau}\rangle_\tau=-\frac{\partial}{\partial a}\langle e^{-a\tau}\rangle_\tau=c\mu a^{\mu-1}e^{-ca^\mu}, \tag{A10}$$

with $c=\Gamma(1-\mu)$, so that $\langle \hat{I}_n(s)\rangle_\tau$ reads

$$\langle \hat{I}_n(s)\rangle_\tau=c\mu[s\mathcal{N}_W(x)]^{\mu-1}\exp\left\{-cs^\mu\left[\sum_{x'}\mathcal{N}_W(x')^\mu\right]\right\}. \tag{A11}$$

Next, one has to average over all the walks W ending on site x in n steps. Since this part is the hardest one of the calculation, one has to resort to a simple approximation scheme, valid in the vicinity of some specific value of μ, namely, μ close to 1 in the following.

a. An approximation for $\mu\to 1$

A simple approximation consists in performing the average $\langle\cdots\rangle_{n,x}$ of the right hand side of Eq. (A11) by replacing $\mathcal{N}_W(x')$ with $\mathcal{N}_x(x',n)=\langle \mathcal{N}_W(x')\rangle_{n,x}$:

$$\begin{aligned}\langle\langle \hat{I}_n(s)\rangle_\tau\rangle_{n,x}&=\left\langle c\mu[s\mathcal{N}_W(x)]^{\mu-1}\right.\\ &\quad\left.\times\exp\left\{-cs^\mu\left[\sum_{x'}\mathcal{N}_W(x')^\mu\right]\right\}\right\rangle_{n,x}\\ &\simeq c\mu[s\mathcal{N}_x(x,n)]^{\mu-1}\\ &\quad\times\exp\left\{-cs^\mu\left[\sum_{x'}\mathcal{N}_x(x',n)^\mu\right]\right\}.\end{aligned} \tag{A12}$$

This approximation is expected to be correct, at large times, for μ close to 1 ($\mu<1$), since it is exact for $\mu=1$. Note however that for $\mu=1$, Eq. (A9) is no longer valid, and logarithmic corrections come into play. Turning to $\mathcal{N}_x(x',n)$, it can be shown that for large n, a scaling relation holds:

$$\mathcal{N}_x(x',n)=\sqrt{n}F\left(\frac{x'}{\sqrt{n}},\frac{x}{\sqrt{n}}\right) \tag{A13}$$

with $F(v,z)$ given by the following integral:

$$F(v,z)=\frac{1}{\sqrt{2\pi}}\int_0^1 \frac{du}{\sqrt{\sin\pi u}} e^{-(v-zu)^2/2\sin\pi u}. \tag{A14}$$

The different factors in Eq. (A12) can then be evaluated:

$$\begin{aligned}\sum_{x'}\mathcal{N}_x(x',n)^\mu&=\int_{-\infty}^{+\infty}\sqrt{n}dv\left[\sqrt{n}F\left(v,\frac{x}{\sqrt{n}}\right)\right]^\mu\\ &=\sqrt{n}^{1+\mu}G\left(\frac{x}{\sqrt{n}}\right)\end{aligned} \tag{A15}$$

introducing $G(z)=\int_{-\infty}^{+\infty}F(v,z)^{\mu}dv$.

$$\mathcal{N}_x(x,n)^{\mu-1}=\sqrt{n}^{\mu-1}F\left(\frac{x}{\sqrt{n}},\frac{x}{\sqrt{n}}\right)^{\mu-1}=\sqrt{n}^{\mu-1}H\left(\frac{x}{\sqrt{n}}\right)^{\mu-1} \tag{A16}$$

with $H(v)=F(v,v)$. From Eq. (A5), a continuous space limit can be obtained, introducing a continuous scaling variable λ through the natural scaling relation $n=\lambda x^2$,

$$\langle\hat{p}(x,s)\rangle_{\tau}=x^2\int_0^{\infty}d\lambda\left[\frac{e^{-1/2\lambda}}{|x|\sqrt{2\pi\lambda}}\right]\times\left[c\mu s^{\mu-1}(|x|\sqrt{\lambda})^{\mu-1}H\left(\frac{1}{\sqrt{\lambda}}\right)^{\mu-1}\right]\times e^{-[cs^{\mu}|x|^{1+\mu}\sqrt{\lambda}^{1+\mu}G(1/\sqrt{\lambda})]}, \tag{A17}$$

where the parity of $G(z)$ and $H(z)$ has been used. Grouping together the factors, and introducing the scaling variable $\eta=|x|^{(1+\mu)/\mu}s$, we get

$$\langle\hat{p}(x,s)\rangle_{\tau}=|x|^{1/\mu}\frac{\mu c}{\sqrt{2\pi}}\eta^{\mu-1}\int_0^{\infty}d\lambda\lambda^{(\mu/2)-1}\times H\left(\frac{1}{\sqrt{\lambda}}\right)^{\mu-1}e^{-(1/2\lambda)-c\eta^{\mu}\lambda^{(1+\mu)/2}G(1/\sqrt{\lambda})}. \tag{A18}$$

Note that this expression is compatible with the expected scaling form

$$\langle p(x,t)\rangle_{\tau}=\frac{1}{\xi}f\left(\frac{|x|}{\xi}\right), \tag{A19}$$

where ξ is the dynamical length scale appearing in the model, $\xi\sim t^{\mu/(1+\mu)}$. One can indeed rewrite the previous relation in the following way:

$$\langle p(x,t)\rangle_{\tau}=\frac{1}{|x|}g\left(\frac{t}{|x|^{(1+\mu)/\mu}}\right). \tag{A20}$$

Taking the Laplace transform with respect to t yields

$$\langle\hat{p}(x,s)\rangle_{\tau}=|x|^{1/\mu}\hat{g}(\eta), \tag{A21}$$

where $\hat{g}$ is the Laplace transform of g, which is of the form Eq. (A18). So one deduces that the scaling function $\hat{g}(\eta)$ is given by

$$\hat{g}(\eta)=\frac{\mu c}{\sqrt{2\pi}}\eta^{\mu-1}\int_0^{\infty}d\lambda\lambda^{(\mu/2)-1}\times H\left(\frac{1}{\sqrt{\lambda}}\right)^{\mu-1}e^{-(1/2\lambda)-c\eta^{\mu}\lambda^{(1+\mu)/2}G(1/\sqrt{\lambda})}. \tag{A22}$$

b. Asymptotic behavior of the scaling function f

Now we focus on the asymptotic behavior of $\hat{g}(\eta)$ for large η, which gives the spatial tails of the distribution $\langle p(x,t)\rangle_{\tau}$. When $\eta\to\infty$, the above integral is dominated by the small λ region, which means that one needs to know the asymptotic large z behavior of $H(z)$ and $G(z)$. After a few lines of computations, we finally find

$$H(z)\simeq\frac{1}{z},\quad G(z)\simeq z^{1-\mu},\quad z\to\infty. \tag{A23}$$

The large η behavior of $\hat{g}(\eta)$ can be then obtained from

$$\hat{g}(\eta)=\frac{\mu c}{\sqrt{2\pi}}\eta^{\mu-1}\int_0^{+\infty}d\lambda\lambda^{\mu-(3/2)}e^{-(1/2\lambda)-c\eta^{\mu}\lambda^{\mu}}. \tag{A24}$$

The inverse Laplace transform can be computed using a saddle-point method. One finally finds for the large $|x|$ behavior [or large $|\zeta|$, with $\zeta=xt^{-\mu/(1+\mu)}$]

$$f(\zeta)\approx f_{\infty}|\zeta|^{(\mu-1)/2}e^{-b|\zeta|^{1+\mu}} \tag{A25}$$

with

$$f_{\infty}=\sqrt{\frac{\mu\Gamma(1-\mu)}{2^{\mu}\pi}},\quad b=2^{-\mu}\Gamma(1-\mu). \tag{A26}$$

One can also look at the limit $\zeta\to 0$. Starting from Eq. (A22), we have to calculate the small z behavior of $G(z)$ and $H(z)$, which is simple here since these function have a finite limit in 0, denoted by $g_0(\mu)$ and h_0, respectively as

$$g_0(\mu)=\int_{-\infty}^{+\infty}dv\left(\frac{1}{\sqrt{2\pi}}\int_0^1\frac{du}{\sqrt{\sin\pi u}}\exp v^2/(2\sin\pi u)\right)^{\mu}, \tag{A27}$$

$$h_0=\frac{1}{\sqrt{2\pi}}\int_0^1\frac{du}{\sqrt{\sin\pi u}}=\frac{\Gamma\left(\frac{1}{4}\right)^2}{2\pi^2}. \tag{A28}$$

So we have to compute the following integral:

$$\hat{g}(\eta)=\frac{\mu c}{\sqrt{2\pi}}h_0^{\mu-1}\eta^{\mu-1}\int_0^{\infty}d\lambda\lambda^{(\mu/2)-1}\times e^{-(1/2\lambda)-cg_0(\mu)\eta^{\mu}\lambda^{(1+\mu)/2}}. \tag{A29}$$

For $\eta\to 0$, this integral is dominated by the large λ region. We finally find

$$\hat{g}(\eta)=A\eta^{-1/(1+\mu)},\quad \eta\to 0, \tag{A30}$$

with

$$A=\frac{1}{\sqrt{2\pi}}\frac{2\mu}{1+\mu}\Gamma(1-\mu)^{1/(1+\mu)}g_0(\mu)^{-\mu/(1+\mu)} \times h_0^{\mu-1}\Gamma\left(\frac{\mu}{1+\mu}\right). \tag{A31}$$

Taking the inverse Laplace transform, this term gives the value of $\langle p(x=0,t)\rangle_\tau$ which is proportional to $t^{-\mu/(1+\mu)}$. In order to get the spatial dependence, the next term of the expansion must be computed. After a few changes of variables and asymptotic estimates, we get

$$f(\zeta)=f_0-f_1|\zeta|^\mu, \quad \zeta\to 0, \tag{A32}$$

with

$$f_0=\frac{2\mu h_0^{\mu-1}}{(1+\mu)\sqrt{2\pi}}g_0(\mu)^{-\mu/(1+\mu)}\frac{\Gamma(1-\mu)^{1/(1+\mu)}\Gamma\left(\frac{\mu}{1+\mu}\right)}{\Gamma\left(\frac{1}{1+\mu}\right)}, \tag{A33}$$

$$f_1=\frac{2^{(1-\mu)/2}}{\sqrt{\pi}}h_0^{\mu-1}\Gamma\left(1-\frac{\mu}{2}\right). \tag{A34}$$

The next subleading term can also be computed, and is found to be of order ζ^2 for $\mu>1/2$, and $\zeta^{1+2\mu}$ for $\mu<1/2$.

APPENDIX B:

We give here some technical details about the numerical simulations. A number N_w of independent ''walkers'' (or ''particles') are simulated one by one, for a given sample of the quenched energies $\{E_i\}$. A walk is simulated as follows: the trapping time on site i is chosen randomly from an exponential distribution of mean $\tau_i=\exp(E_i/T)$, and the walker then chooses at random between the two neighboring sites, with equal probability. Then the desired quantity is computed for this particular sample, and eventually averaged over a number N_s of samples. Moreover, in order to facilitate comparisons between different runs, we took each time the same disorder samples, by choosing the same set of ''seed'' numbers. For out of equilibrium simulations, where the number of sites $L=2N+1$ is supposed to be infinite, we used periodic boundary conditions, with usually $N=10^3$ except when long times were required, in which case $N=10^4$ was instead considered [for instance in the computation of $Y_k(t)$].

Error bars are estimated by running several simulations with the same N_w and N_s, varying only the seed numbers. The fluctuations between the different runs leads to an estimate of the standard deviation. The numbers N_w and N_s were chosen so as to get small enough error bars, as far as possible, taking into account the time t that we need to reach as well as the computational time. It should be emphasized that the amplitude of the fluctuations depends a lot on the computed quantity. Correlations functions are easy to compute, and $N_w=N_s=10^3$ is enough to get a relative standard deviation which is less than 10^{-2}. Quantities related to localization properties fluctuate more; for integrated quantities like the participation ratios, we took $N_w=10^3$ and $N_s=10^4$ (except for small size systems, where $N_w=N_s=2\times10^3$ was used instead), which was a good compromise in order to obtain both a good standard deviation (less than 10^{-2}) and long enough times (for instance $t=10^6$ for $\mu=0.5$). For distributions like $\varphi(P)$ and $\langle p(x,t)\rangle$, one needs to average over a larger number of samples, in order to get smooth enough curves (with fluctuations between different runs less than 5×10^{-2}). So $\varphi(P)$ was simulated using $N_w=10^4$ and $N_s=10^5$, whereas $\langle p(x,t)\rangle$ was computed with $N_w=10^3$ and $N_s=10^5$. Note finally that $Y_2(\ell,t)$ was simulated using $N_w=10^5$, and $N_s=10^3$ (except for $t=10^6$ and 10^7, where $N_w=5\times10^4$ and 10^4, respectively), since we need a good statistics on the sites with small trapping times so as to avoid large fluctuations at small ℓ.

APPENDIX C: CALCULATION OF THE PARTICIPATION RATIOS

The analytical calculation of $Y_2(t)$ appears not to be easily tractable, and the aim of this appendix is to argue for the existence of a finite limit Y_2^{dyn} of $Y_2(t)$ when $t\to\infty$ for $\mu<1$, and try to extract some information on the behavior of Y_2^{dyn} as a function of μ, in particular for μ close to 1.

The participation ratio $Y_2(t)$ is given by the integral $\int_{-\infty}^{+\infty}\langle p(x,t)^2\rangle_\tau$. The quantity $\langle p(x,t)^2\rangle_\tau$ can be computed following the same lines as for $\langle p(x,t)\rangle_\tau$. It will be useful to introduce a two-time quantity $Q(x,t,t')$ defined as

$$Q(x,t,t')=\langle p(x,t)p(x,t')\rangle_\tau. \tag{C1}$$

Defining $R(t,t')=\int_{-\infty}^{\infty}dx\,Q(x,t,t')$, one has $Y_2(t)=R(t,t)$, and turning to the Laplace transform

$$\hat{R}(s,s')=\int_0^\infty dt\int_0^\infty dt' e^{-st-s't'}R(t,t'). \tag{C2}$$

Now a reasonable assumption (that has been checked numerically) is that for large t and t', $t>t'$, $R(t,t')$ becomes a function of t/t',

$$R(t,t')=Y_2^{dyn}\mathcal{R}\left(\frac{t}{t'}\right). \tag{C3}$$

This follows from the similar behavior of the correlation function $C(t,t')$ studied in Sec. V. It is interesting to restrict to the particular case $s=s'$,

$$\hat{R}(s,s)=2Y_2^{dyn}\int_0^\infty dt'\int_t^{'\infty}dte^{-s(t+t')}\mathcal{R}\left(\frac{t}{t'}\right) =2Y_2^{dyn}\int_0^\infty dt'\int_1^\infty dut'e^{-st'(1+u)}\mathcal{R}(u) \tag{C4}$$

or

$$\hat{R}(s,s)=\frac{2Y_2^{dyn}}{s^2}\int_1^\infty du\frac{\mathcal{R}(u)}{(1+u)^2}. \tag{C5}$$

So a finite limit for $Y_2(t)$ corresponds to $\hat{R}(s,s)\sim s^{-2}$, and this is what we shall try to show in the following. Coming back to $Q(x,t,t')$ and decomposing over the number of steps, one has

$$Q(x,t,t')=\sum_{n,n'} p(x,n,t)p(x,n',t'). \tag{C6}$$

Averaging over the disorder yields

$$\begin{aligned}\langle Q(x,t,t')\rangle_\tau=&\sum_{n,n'} q(x|n)q(x|n')\\ &\times\langle I(t_n<t<t_{n+1})\\ &\times I(t'_{n'}<t'<t'_{n'+1})\rangle_{\tau,(n,x),(n',x)}.\end{aligned} \tag{C7}$$

For given walks W and W', and a given sequence of τ_i, let us introduce $\hat{K}_{n,n'}(s,s')$ defined by

$$\begin{aligned}\hat{K}_{n,n'}(s,s')=&\int_0^\infty dt\int_0^\infty dt' I(t_n<t<t_{n+1})\\ &\times I(t'_{n'}<t'<t'_{n'+1})e^{-st-s't'}\\ \simeq&\tau(x)^2e^{-st_n-s't'_{n'}}\end{aligned} \tag{C8}$$

assuming again that $t_{n+1}-t_n=t'_{n'+1}-t'_{n'}=\tau(x)$ (i.e., trapping times are fixed rather than exponentially distributed) and that $s\tau(x)$ and $s'\tau(x)$ are both much smaller than 1, which means that the maximum trapping time encountered is much smaller than the times t and t' considered. Introducing the following decomposition:

$$t_n=\sum_y \mathcal{N}_W(y,n)\tau(y), \tag{C9}$$

$$t'_{n'}=\sum_y \mathcal{N}_{W'}(y,n')\tau(y), \tag{C10}$$

$\hat{K}_{n,n'}(s,s')$ reads

$$\begin{aligned}\hat{K}_{n,n'}(s,s')=&\tau(x)^2e^{-[s\mathcal{N}_W(x,n)+s'\mathcal{N}_{W'}(x,n')]\tau(x)}\\ &\times\prod_{y\neq x} e^{-[s\mathcal{N}_W(y,n)+s'\mathcal{N}_{W'}(y,n')]\tau(y)}.\end{aligned} \tag{C11}$$

Averaging $\hat{K}_{n,n'}(s,s')$ over the disorder, one has

$$\begin{aligned}\langle\hat{K}_{n,n'}(s,s')\rangle_\tau=&\mu\Gamma(2-\mu)\times[s\mathcal{N}_W(x,n)\\ &+s'\mathcal{N}_{W'}(x,n')]^{\mu-2}\\ &\times\prod_{y\neq x} e^{-c[s\mathcal{N}_W(y,n)+s'\mathcal{N}'_{W'}(y,n')]^\mu}.\end{aligned} \tag{C12}$$

One can now write $\hat{R}(s,s)$ as

$$\begin{aligned}\hat{R}(s,s)=&2\mu\Gamma(2-\mu)\sum_x\sum_{n<n'} q(x|n)q(x|n')s^{\mu-2}\\ &\times[\mathcal{N}_W(x,n)+\mathcal{N}_{W'}(x,n')]^{\mu-2}\exp\Bigg\{-cs^\mu\\ &\times\sum_y[\mathcal{N}_W(y,n)+\mathcal{N}_{W'}(y,n')]^\mu\Bigg\}.\end{aligned} \tag{C13}$$

We now turn to continuous limit, and replace as in Appendix A $\mathcal{N}_W(y,n)$ by its average value $\sqrt{n}F(y/\sqrt{n},x/\sqrt{n})$. At this stage we drop order unity constants since we shall make several rather crude approximations in the following. Introducing the new variable β through $n'=\beta n$, one gets

$$\begin{aligned}\hat{R}(s,s)\sim&s^{\mu-2}\int_{-\infty}^\infty dx\int_1^\infty dn\int_1^\infty\frac{d\beta}{\sqrt{\beta}}e^{-(x^2/2n)(1+1/\beta)}\\ &\times\left[\sqrt{n}H\left(\frac{x}{\sqrt{n}}\right)+\sqrt{\beta n}H\left(\frac{x}{\sqrt{\beta n}}\right)\right]^{\mu-2}\\ &\times\exp\Bigg\{-cs^\mu\int_{-\infty}^\infty dy\,n^{\mu/2}\Bigg[F\left(\frac{y}{\sqrt{n}},\frac{x}{\sqrt{n}}\right)\\ &+\sqrt{\beta}F\left(\frac{y}{\sqrt{\beta n}},\frac{x}{\sqrt{\beta n}}\right)\Bigg]^\mu\Bigg\}.\end{aligned} \tag{C14}$$

Now, because of the factor $1/\sqrt{\beta}$, the integral over β is dominated by the large β behavior, which means that as a first step one can neglect terms like $F(y/\sqrt{n},x/\sqrt{n})$ compared to $\sqrt{\beta}F(y/\sqrt{\beta n},x/\sqrt{\beta n})$. Rescaling also x and y using the new variables $\hat{x}=x/\sqrt{n}$ and $\hat{y}=y/\sqrt{\beta n}$ yields

$$\begin{aligned}\hat{R}(s,s)\sim&s^{\mu-2}\int_{-\infty}^\infty d\hat{x}\int_1^\infty d\beta\beta^{(\mu-3)/2}\int_1^\infty dn\,n^{(\mu-1)/2}\\ &\times e^{-(\hat{x}/2)(1+1/\beta)}H\left(\frac{\hat{x}}{\sqrt{\beta}}\right)^{\mu-2}e^{-cs^\mu(\beta n)^{(1+\mu)/2}G(\hat{x}/\sqrt{\beta})}.\end{aligned} \tag{C15}$$

One can change variable in the last integral over n, letting

$$n=\frac{1}{\beta s^{2\mu/(1+\mu)}}\left[\frac{v}{c\,G\left(\dfrac{\hat{x}}{\sqrt{\beta}}\right)}\right]^{2/(1+\mu)}. \tag{C16}$$

Then the integral over v becomes $\int_0^\infty dv\, e^{-v}=1$ (for $s\to 0$), and $\hat{R}(s,s)$ reduces to

$$\hat{R}(s,s)\sim\frac{1}{cs^2}\int_1^\infty\frac{d\beta}{\beta^2}\int_{-\infty}^{\infty}d\hat{x}\,e^{-(\hat{x}/2)(1+1/\beta)}\frac{H\left(\dfrac{\hat{x}}{\sqrt{\beta}}\right)^{\mu-2}}{G\left(\dfrac{\hat{x}}{\sqrt{\beta}}\right)}. \tag{C17}$$

So this simplified calculation is consistent with a finite Y_2^{dyn} given by

$$Y_2^{dyn}\propto\frac{1}{\Gamma(1-\mu)}\int_1^\infty\frac{d\beta}{\beta^2}\int_{-\infty}^{\infty}d\hat{x}\,e^{-(\hat{x}/2)(1+1/\beta)}\frac{H\left(\dfrac{\hat{x}}{\sqrt{\beta}}\right)^{\mu-2}}{G\left(\dfrac{\hat{x}}{\sqrt{\beta}}\right)}, \tag{C18}$$

where we have used $c=\Gamma(1-\mu)$.

Since $\lim_{z\to 0}G(z)=g_0(\mu)\to 1$ when $\mu\to 1$ and $\lim_{z\to 0}H(z)=h_0$ is independent of μ, the only strong dependence upon μ comes from $\Gamma(1-\mu)$, which suggests that

$$Y_2^{dyn}\sim(1-\mu),\quad \mu\to 0. \tag{C19}$$

This results is compatible with numerical data, and is comparable to the corresponding result in equilibrium (in this case, $Y_2^{eq}=1-\mu$ for all $\mu<1$). For $1<\mu<2$, one can easily show that, under the same assumptions, $Y_2(t)\sim 1/t^{(\mu-1)/2}$ when $t\to\infty$, whereas $Y_2(t)\sim 1/\sqrt{t}$ for $\mu>2$, which is the expected result. Turning to Y_3, we have checked that the same calculation also leads to a finite limit, and to a linear behavior with respect to μ when $\mu\to 1$.

[1] L.C.E. Struick, *Physical Aging in Amorphous Polymers and Other Materials* (Elsevier, Houston, 1978).
[2] E. Vincent, J. Hammann, M. Ocio, J.-P. Bouchaud, and L.F. Cugliandolo: in *Proceeding of the Sitges Conference on Glassy Systems*, edited by E. Rubi (Springer-Verlag, Berlin, 1996).
[3] J.-P. Bouchaud, L. Cugliandolo, J. Kurchan, M. Mézard, in *Spin Glasses and Random Fields*, edited by A.P. Young (World Scientific, Singapore, 1998), and references therein.
[4] J.-P. Bouchaud, J. Phys. I **2**, 1705 (1992).
[5] B. Doliwa and A. Heuer, e-print cond-mat/0209139.
[6] R.A. Denny, D.R. Reichman, and J.-P. Bouchaud, e-print cond-mat/0209020.
[7] L. Berthier, e-print cond-mat/0209394.
[8] P. Sollich, F. Lequeux, P. Hebraud, and M.E. Cates, Phys. Rev. Lett. **78**, 2020 (1997).
[9] S.M. Fielding, P. Sollich, and M.E. Cates, J. Rheol. **44**, 323 (2000).
[10] D.A. Head, Phys. Rev. E **62**, 2439 (2000).
[11] L. Balents, J.-P. Bouchaud, and M. Mézard, J. Phys. I **6**, 1007 (1996).
[12] J.C. Dyre, Phys. Rev. Lett. **58**, 792 (1987); Phys. Rev. B **51**, 12 276 (1995).
[13] J.-P. Bouchaud and D.S. Dean, J. Phys. I **5**, 265 (1995).
[14] C. Monthus and J.-P. Bouchaud, J. Phys. A **29**, 3847 (1996).
[15] G. Ben Arous, A. Bovier, and V. Gayrard, Phys. Rev. Lett. **88**, 087201 (2002).
[16] S. Fielding and P. Sollich, Phys. Rev. Lett. **88**, 050603 (2002).
[17] L.F. Cugliandolo and J. Kurchan, J. Phys. A **27**, 5749 (1994).
[18] E. Bertin and J.-P. Bouchaud, J. Phys. A **35**, 3039 (2002).
[19] T.S. Grigera and N. Israeloff, Phys. Rev. Lett. **83**, 5038 (1999).
[20] L. Cipelletti, H. Bissig, V. Trappe, P. Ballestat, and S. Mazoyer, J. Phys: Cond. Mat. (to be published).
[21] L. Buisson, L. Bellon, and S. Ciliberto (unpublished).
[22] F. Bardou, J.P. Bouchaud, A. Aspect, and C. Cohen-Tannoudji, *Lévy Statistics and Laser Cooling* (Cambridge University Press, Cambridge, England, 2002).
[23] Y. Jung, E. Barkai, and R.J. Silbey, Chem. Phys. **284**, 181 (2002) (special issue S1 Nov 1).
[24] X. Brokmann, J.-P. Hermier, G. Messin, P. Desbiolles, J.-P. Bouchaud, and M. Dahan, e-print cond-mat/0211171.
[25] S. Alexander, Phys. Rev. B **23**, 2951 (1981).
[26] S. Alexander, J. Bernasconi, W.R. Schneider, and R. Orbach, Rev. Mod. Phys. **53**, 175 (1981); and in *Physics in One Dimension*, edited by J. Bernasconi and T. Schneider (Springer-Verlag, Berlin, 1981).
[27] J. Machta, J. Phys. A **18**, L531 (1985).
[28] J.-P. Bouchaud and A. Georges, Phys. Rep. **195**, 127 (1990).
[29] B. Rinn, P. Maass, and J.-P. Bouchaud, Phys. Rev. B **64**, 104417 (2001).
[30] L.R.G. Fontes, M. Isopi, and C.M. Newman, Ann. Prob. **30**, 579 (2002).
[31] G. Ben Arous, in *Proceedings of International Congress of Mathematicians, Beijing 2002* (unpublished), Vol. III, pp. 1–12, and references therein.
[32] A. Golosov, Chem. Phys. **92**, 491 (1984).
[33] A. Compte and J.-P. Bouchaud, J. Phys. A **31**, 6113 (1998).
[34] P. Le Doussal, Thesis, Univ. Paris 6, 1987.
[35] J.-P. Bouchaud, A. Georges, and P. Le Doussal, J. Phys. (France) **48**, 1855 (1987).
[36] H. Yoshino, K. Hukushima, and H. Takayama, Prog. Theor. Phys. Suppl. **126**, 107 (1997).
[37] S. Franz and M.A. Virasoro, J. Phys. A **33**, 891 (2000).
[38] A. Barrat and L. Berthier, Phys. Rev. Lett. **87**, 087204 (2001).
[39] See, e.g., Y.M. Blanter and A.D. Mirlin, Phys. Rev. E **55**, 6514 (1997), and references therein.
[40] M. Mézard, G. Parisi, and M.A. Virasoro, *Spin Glass Theory and Beyond* (World Scientific, Singapore, 1987).

[41] B. Derrida, Physica D **107**, 186 (1997).
[42] J.P. Bouchaud and M. Potters, *Theory of Financial Risks* (Cambridge University Press, Cambridge, England, 2000), Chap. 3.
[43] M. Mézard, G. Parisi, N. Sourlas, G. Toulouse, and M. Virasoro, J. Phys. (France) **45**, 843 (1984).
[44] J.-P. Bouchaud and M. Mézard, J. Phys. A **31**, 6113 (1998).
[45] C. Monthus and P. Le Doussal, Phys. Rev. E **65**, 066129 (2002).
[46] E.M. Bertin, J.-P. Bouchaud (unpublished).